

1 **Tight oil sandstones in Upper Triassic Yanchang Formation, Ordos**
2 **Basin, N. China: Reservoir quality destruction in a closed diagenetic**
3 **system**

4

5 Mingjie Liu¹, Jon Gluyas², Weibin Wang^{3, 4}, Zhen Liu⁵, Junbang Liu⁶, Xiucheng Tan¹, Wei Zeng¹,
6 Yi Xiong⁷

7

8 ¹ School of Geoscience and Technology, Southwest Petroleum University, Chengdu, 610500, China

9 ² Department of Earth Sciences, Durham University, Durham, DH1 3LE, UK

10 ³ Research Institute of Exploration and Development, PetroChina Changqing Oil Field Company, Xi'an 710018,
11 China

12 ⁴ National Engineering Laboratory for Exploration and Development of Low-Permeability Oil & Gas Fields,
13 PetroChina, Xi'an 710018, China

14 ⁵ College of Geosciences, China University of Petroleum, Beijing, 102249, China

15 ⁶ Research Institute of Petroleum Exploration and Development, PetroChina, Beijing 100083, China

16 ⁷ School of Geosciences, Yangtze University, Wuhan, 430100, China

17

18 **Correspondence**

19 Mingjie Liu, School of Geoscience and Technology, Southwest Petroleum University, No. 8, Xindu Road, Xindu
20 District, Chengdu 610500, China. E-mail: liumingjieldd@163.com

21 **Funding information.** Natural Science Foundation of China (Grant No. 41502147, Grant No. 41672124), China
22 Postdoctoral Science Foundation (Grant No. 2016M600752), Sichuan Province Education Department Foundation
23 (Grant No. 16ZA0072), National science and technology major project of China (Grant No.
24 2016ZX05047001-002)

25

26 **ABSTRACT**

27 An investigation of the Triassic Yanchang Formation, Ordos Basin, N. China, revealed
28 that the diagenesis and quality of tight oil sandstone reservoirs (with an average
29 porosity of 9.83% and an average permeability of 0.96 mD) were controlled by a

30 closed diagenetic system. The carbonate cements observed in the sandstone were
31 derived from decarboxylation of organic matter that occurred in the adjacent
32 mudstones. These reactions supplied CO_3^{2-} which reacted with cations derived from
33 grain dissolution in the sandstones. The average size of the diagenetic geochemical
34 system with respect to carbonate cements was small ($<6 \times 10^{-2} \text{m}^3$), comprising
35 sandstone and its adjacent mudstone(s). The carbonate cements tend to concentrate in
36 the marginal sandstone which is taken to indicate that the flux of CO_3^{2-} into the
37 sandstones limited the quantity of carbonate precipitated. In addition, the mass near
38 balance between the amount of feldspar dissolution and its byproducts in the central
39 sandstone (distance to the sandstone/mudstone interface is mainly more than 1 m),
40 where the permeability of sandstone will present a decrease trend with the increasing
41 of feldspar dissolution pores. The pore space of central sandstone will be just
42 redistributed, with primary intergranular pores converting to feldspar dissolution
43 pores and clay minerals micropores. Thus, the best part of the sandstone reservoirs
44 tends to be the central part of sandstone. In particular, sandstones that are more than 2
45 m thick could be the potential hydrocarbon reservoirs because they retain the best
46 porosity (average of 13.6%) and permeability (average of 1.8 mD). The results of our
47 study provide an important guide for the exploration of tight oil sandstones in other
48 petroliferous basins over the world.

49

50 **KEYWORDS**

51 closed diagenetic geochemical system; Ordos Basin; reservoir quality; tight oil
52 sandstone; Yanchang Formation

53 **1 INTRODUCTION**

54 It is now widely believed that the quality of sandstone reservoir is controlled by the
55 original depositional characteristics and diagenesis (Dutton & Loucks, 2010;
56 Ehrenberg, 1990; Gluyas & Coleman, 1992; Higgs, Zwingmann, Reyes, & Funnell,
57 2007; Mansurbeg et al., 2009; Morad, Ketzer, & DeRos, 2000; Taylor et al., 2010).
58 Various integrated approaches and cases have been given to analyze how the

59 sandstone reservoir quality is controlled by the diagenesis (Gier, Worden, Jones, &
60 Kurzweil, 2008; Maast, Jahren, & Bjørlykke, 2011; Umar, Friis, Khan, Kassi, & Kasi,
61 2011; Yuan et al., 2015a; Zhang, Pe-piper, & Piper, 2015). However, most of the
62 studies are based mainly on the description of diagenesis, with only a little
63 consideration given to the geochemical constraints on the diagenetic system
64 (Bjørlykke & Jahren, 2012; Chuhan, Bjørlykke, & Lowrey, 2001; Yuan et al., 2015b;
65 Yuan, Cao, Zhang, & Gluyas, 2017). Essentially, the dissolution and precipitation of
66 minerals are chemical reactions, with their extent and rates controlled by a
67 combination of temperature, pore-water composition and some parameters such as
68 redox potential (Eh) and acidity (pH). These processes make up the “the geochemical
69 system”, which can be divided into open system and closed system according to the
70 exchange characteristics of diagenetic materials (Bjørlykke & Jahren, 2012).
71 Although some detailed papers have been published to investigate the relationship
72 between the open/closed geochemical system and diagenesis, their mainly focused on
73 the conventional sandstone and mudstone, not including the tight sandstone
74 (Bjørlykke & Jahren, 2012; Chuhan et al., 2001; Day-Stirrat et al., 2010; Yuan et al.,
75 2015b; 2017).

76 As one of the most important unconventional hydrocarbon resources, the tight
77 sandstones have been found widely distributed in the petroliferous basins of the world
78 in recent decades (Higgs et al., 2007; Schmitt et al., 2015; Spencer, 1985), especially
79 in China, such as the Ordos Basin, Sichuan Basin, Bohai Bay Basin and Songliao
80 Basin (Liu et al., 2014; Liu, Liu, Wu, Zhu, & Wang, 2017; Xi et al., 2015a; Zou et al.,
81 2012a). Generally, a tight sandstone is defined as a sandstone with porosity lower
82 than 10%, the air permeability lower than 1mD (Law & Curtis, 2002; Spencer, 1985;
83 Stroker, Harris, Crawford Elliott, & Marion Wampler, 2013; Xi et al., 2015a ; Zou et
84 al., 2010a). The Upper Triassic Yanchang Formation is a prolific oil-producing unit of
85 the Ordos Basin (Fu et al., 2017; Guo et al., 2012; Yang, Li, & Liu, 2013; Yao et al.,
86 2013). Diagenesis of the tight sandstone in Yanchang Formation has been reported in
87 some published works, most of which are focused on the Chang 7 Member (e.g., Cui
88 et al., 2017; Dou, Liu, Wu, Xu, & Feng, 2017; Wu et al., 2016; Zhang, Bao, Zhao,

89 Jiang, & Gong, 2017; Zhu et al., 2015). However, limited attention has been paid to
90 the Chang 8 Member (Liu, Liu, Wang, & Pan, 2016; Wang, Chang, Yin, Li, & Song,
91 2017; Zhou et al., 2016), as well as the relationship between diagenesis and reservoir
92 quality based on the diagenetic geochemical system. Additionally, although the
93 effects of diagenetic alterations have been well studied to provide valuable
94 interpretations for tight sandstone reservoir quality, difficulties remain when applying
95 the present results to predict the “sweet zones” of anomalously high porosity and
96 permeability within the tight sandstone reservoirs of Chang 8 Member.

97 The good core coverage of tight oil sandstone in Xifeng oilfield provides an
98 excellent opportunity to investigate this problem. In this paper, we take a combined
99 analysis of petrography, porosity and permeability, stable isotopic compositions of
100 authigenic minerals, homogenization temperature and final ice melting temperature of
101 aqueous fluid inclusion and pore water chemistry, aimed to: (1) investigate a detailed
102 diagenetic analysis and reconstruct the diagenetic history of Chang 8 Member tight
103 sandstone; (2) identify the type of diagenetic geochemical system; and (3) analyze the
104 control of the diagenetic geochemical system on the tight sandstone reservoir quality
105 in Chang 8 Member.

106 **2 GEOLOGICAL BACKGROUND**

107 The Ordos Basin, as the second largest sedimentary basin in China, locates in the
108 western part of the North China Block and covers approximately 320 000 km² (Figure
109 1 A) (Liu et al., 2004; Yang, Jin, Van Loon, Han, & Fan, 2017). It is a typical cratonic
110 basin characterized by gentle, west-dipping monocline with dip angles less than 1°
111 (Figure 1 B) (He, 2003; Liu et al., 2014; Wang et al., 2017). Six first-order tectonic
112 units in the Ordos Basin have been identified, i.e., the Yimeng Uplift in the north, the
113 Western Thrust Belt on the west margin, the Tianhuan Depression in the west, the
114 Yishan Slope in the center, the Weibei Uplift in the south and the Jinxi Fault-Fold
115 Belt in the east (Figure 1 C) (Liu et al., 2016; Yang, 2002). The studied Xifeng Area,
116 as one of the most oil-rich areas, belongs to the Yishan Slope and locates in the

117 south-western part of the Ordos Basin. Based on the filling sequence and structures,
118 the Ordos Basin evolution can be divided into five stages: (1) an aulacogen stage
119 during the Middle-Late Proterozoic, (2) a shallow oceanic platform stage during the
120 Early Palaeozoic, (3) an offshore plain stage during the Late Palaeozoic, (4) a
121 lacustrine basin stage during the Mesozoic, and (5) a peripheral fault depression stage
122 during the Cenozoic (Xu et al., 2017; Yang, Liu, Zhang, Han, & Hui, 2007).

123 During the Late Triassic, the Yanchang Formation is dominated by fluvial,
124 lacustrine and deltaic sedimentation with a thickness of 1000–1300 m throughout
125 most of the Ordos Basin (Figure 2) (Cui et al., 2017; Qiu, Liu, Wang, Deng, & Mao,
126 2015; Zou, Wang, Li, Tao, & Hou, 2012b). Recent hydrocarbon exploration and
127 outcrop studies have demonstrated that shallow-lacustrine sand-rich deltas developed
128 extensively along the gentle slopes and central part of the basin, forming the main
129 reservoir rocks of the Triassic oil fields (Zhou et al., 2016). The vertical facies
130 succession indicates that the Yanchang Formation covers the entire lacustrine life
131 cycle of the Late Triassic Ordos Basin (Figure 2) (Zou et al., 2010b).

132 Based on the sedimentary cycle, rock associations, tuff marker beds and log
133 characteristics, the Yanchang Formation is divided into ten members, numbered from
134 top to bottom as Chang 1 to Chang 10 (Figure 2) (He, 2003; Yang, 2002; Yang et al.,
135 2017). Lake-basin development peaked during the deposition of Chang 7 Member,
136 simultaneously peaked in the development of Mesozoic hydrocarbon source rocks
137 with an average total organic carbon (TOC) of 13.75% and a vitrinite reflectance (R_o)
138 in the range of 0.85–1.15% (Yang & Zhang, 2005; Zhang, Yang, Li, & Ma, 2006).
139 The overlying Chang 6 Member and underlying Chang 8 Member are the main
140 reservoir beds of Yanchang Formation tight sandstone hydrocarbon reservoirs (Liu et
141 al., 2014; Zhang, Yang, Hou, & Liu, 2009). This study focused on the Chang 8
142 Member of Xifeng Area, in which oil is mainly accumulated in the sandstones of
143 shallow lacustrine delta distributary channel (Zhou et al., 2016).

144 Burial history and thermal history of the Xifeng Area have been analyzed in
145 detail using data from exploration and production wells and the histories synthesized
146 with the BasinMod software by previous studies (Guo et al., 2012; Liu et al., 2013;

147 Ren et al., 2007). The current geothermal gradient is about 29.3 °C/km, with an
148 average surface temperature of 10.8 °C. Presently, the Yanchang Formation is not at
149 its maximum depth (~3 km) and temperature (130 °C).

150 **3 DATABASES AND METHODS**

151 This study involved the analysis of 268 thin-section samples from 60 wells, 1073
152 reservoir porosity and permeability measurements and 40 formation water data.
153 Samples and data were collected from the PetroChina Research Institute of Petroleum
154 Exploration & Development and PetroChina Changqing Oilfield Company.

155 All the sandstone samples were selected from the Chang 8 Member drill cores of
156 60 wells according to the study objectives and constraints of the collected data. A total
157 of 158 thin sections and 110 blue epoxy resin-impregnated thin sections were
158 prepared for the analysis of rock mineralogy, diagenesis and visual porosity. Thin
159 sections were partly stained with Alizarin Red S and K-ferricyanide for carbonate
160 mineral identification. Point counts were performed on thin sections for the content of
161 detrital grains with at least 300 points, following the method of Yuan et al. (2015a, b).
162 20 micrographs for each of 59 blue epoxy resin-impregnated thin sections were taken
163 using the Leica microscope in the Key Laboratory of Natural Gas Geology of
164 Southwest Petroleum University, Sichuan Province, in order to determining the
165 content of quartz cement, carbonate cements, authigenic clays, primary pores and the
166 feldspar dissolution pores. Objectives of 100× for these thin sections were used, and
167 each micrograph has an area of 6.45mm² (Xi et al., 2015a, b). Then cements and pores
168 in each micrograph were identified under the microscope and sketched by using the
169 CorelDRAW software on computer. The total area of cements and pores in every
170 micrograph was obtained using the Image-Pro Plus software. Finally, the percentages
171 of cements and pores were calculated by taking the average of all values in the 20
172 micrographs for each thin section. Besides, a total of 59 sandstone samples were
173 analyzed for whole-rock (bulk) and clay fraction (<2 μm) mineralogy using XRD in
174 the State Key Laboratory of Oil and Gas Reservoir Geology and Exploitation of

175 Southwest Petroleum University.

176 59 typical samples were identified using a Quanta 250 FEG scanning electron
177 microscope (SEM) equipped with an energy dispersive X-ray spectrometer (EDX) in
178 the State Key Laboratory of Oil and Gas Reservoir Geology and Exploitation of
179 Southwest Petroleum University. Cathodoluminescence (CL) analyses of 14
180 representative samples were made using a Leica microscope equipped with a
181 CL8200-MK5 CL instrument in the Key Laboratory of Natural Gas Geology of
182 Southwest Petroleum University, Sichuan Province. Twenty core samples from 20
183 wells were prepared as thick doubly-polished thin sections for fluid inclusion
184 petrographic analysis and microthermometric measurements in the Key Laboratory of
185 Natural Gas Geology of Southwest Petroleum University, Sichuan Province. The
186 microthermometry of fluid inclusions was studied using a petrographic microscope
187 equipped with a Linkam THMSG 600 heating and cooling stage which enables to
188 transfer the temperatures of phase in the range of -180 to 500 °C. The measured
189 precision for the homogenization temperature (T_h) and ice melting temperature (T_m)
190 are ± 1 °C and ± 0.1 °C, respectively.

191 Based on the petrological studies, 59 organic matter-free sandstone samples were
192 chosen for carbon and oxygen stable isotope analysis. These samples were analyzed
193 using a Thermo-Finnigan MAT 253 isotope ratio mass spectrometer in the Key
194 Laboratory of Natural Gas Geology of Southwest Petroleum University, Sichuan
195 Province, with measured precision was $\pm 0.08\text{‰}$ for O and $\pm 0.06\text{‰}$ for C. Carbon and
196 oxygen stable isotope data are reported in parts per thousand relative to the Vienna
197 PeeDee Belemnite (V-PDB) standards.

198 **4 RESULTS**

199 **4.1 Reservoir lithologies**

200 Petrographic investigation of the tight sandstones in Chang 8 Member shows that the
201 detrital components contain 18.7–64.3% quartz (avg. 38.3%), 5.4–56.5% feldspars
202 (avg. 31.5%) and 5.2–63.1% rock fragments (avg. 30.2%), mostly lithic arkoses and

203 feldspathic litharenites (Figure 3). In the studied tight sandstones, the majority of the
204 detrital quartz grains are monocrystalline. The detrital feldspars are mainly
205 plagioclase and altered K-feldspar. The rock fragments primarily consist of volcanic
206 rock fragments with an average of 19.4%, sedimentary rock fragments with an
207 average of 2.8%, metamorphic rock fragments with an average of 6.7%, and mica
208 with an average of 1.3%. According to the grading analysis, the studied tight
209 sandstones in Chang 8 Member are fine-medium grained, with moderate to well
210 sorting, and the roundness of detrital grains varies from subangular to subrounded.
211 The grain contacts are dominated by linear contacts and concavo-convex contacts.

212 **4.2 Reservoir properties**

213 In general, the reservoir properties of the tight sandstones in Chang 8 Member are
214 quite poor. It decreases with increasing burial depth from 1500 m to 3000 m (Figure
215 4A, B), with the porosity and permeability showing a positive correlation relationship
216 (Figure 4C). The tight sandstones in Chang 8 Member have a range of porosity from
217 1.2% to 18.74% (mainly 4.0% to 16.0%) with an average of 9.83% (Figure 4D).
218 Horizontal permeability ranges from 0.003 to 56.29 mD (mainly less than 1 mD) with
219 an average of 0.96 mD (Figure 4E).

220 **4.3 Diagenetic mineralogy**

221 Authigenic minerals in the tight sandstones of Chang 8 Member mainly consist of
222 quartz, carbonate cements and clay minerals. The authigenic quartz and clays are
223 usually associated with altered feldspar.

224 **4.3.1 Quartz cement**

225 Authigenic quartz is evident in the thin sections and SEM, mainly occurring in two
226 different types of morphologies: quartz overgrowths and authigenic quartz crystals.
227 The quartz overgrowths are easy to discriminate from the detrital grains, with the dust
228 clay rims on the grains in thin sections (Figure 5A) and the euhedral hexagonal
229 pyramid quartz crystal on the grains in SEM (Figure 5B). The authigenic quartz

230 crystals can be identified by the intergranular pore-filling euhedral hexagonal pyramid
231 quartz crystal both in thin sections and SEM (Figure 5C, D). In the studied tight
232 sandstone, the authigenic quartz is difficult to distinguish from the detrital quartz in
233 CL, due to the quartz grain and quartz cement all are dark non-luminescent (Figure 5E,
234 F). As a whole, the authigenic quartz in the tight sandstones of Chang 8 Member was
235 no more than 1% of the whole rock and showed insignificant trend with the burial
236 depth increasing (Figure 6A).

237 **4.3.2 Feldspar dissolution**

238 The feldspar dissolution, especially detrital K-feldspar, is common in the tight
239 sandstone reservoirs of Chang 8 Member, resulting in the formation of significant
240 secondary intragranular pores during the burial stage (Figure 5G). Generally, feldspar
241 dissolution is always accompanied by the precipitation of albite, authigenic quartz
242 crystal and illite (Figure 5H, I), which are the byproducts of feldspar dissolution. The
243 absolute contents of feldspar dissolution obtained from the thin sections ranges from
244 0.81% to 3.63% (avg. 1.78%) of the whole rock, showing no significant trend with
245 increasing burial depth (Figure 6B).

246 **4.3.3 Carbonate cements**

247 Four types of carbonate cements (calcite, dolomite, ferrocalcite and ankerite) have
248 been identified in the tight sandstone of Chang 8 Member. Calcite cements and
249 dolomite cements mainly occur as pore-filling blocky crystals between detrital grains
250 (Figure 7A), and the calcite cements also show a bright orange luminescence color in
251 CL (Figure 7B, C). In addition, the dolomite cements occur as scattered euhedral
252 rhombs and partly fill the intergranular pores (Figure 7D). In thin sections, the
253 ferrocalcite cements and ankerite cements also occur as pore-filling blocky crystals.
254 They mainly filled in the pores around the euhedral authigenic quartz crystal (Figure
255 7E, F), replaced the quartz grain and dolomite cements (Figure 7F-H) and filled the
256 feldspar dissolution pores completely (Figure 7H, I). It indicated that the ferrocalcite
257 and ankerite cements formed after the quartz cement, dolomite cement and feldspar

258 dissolution. As a whole, the content of carbonate cements in the tight sandstone
259 reservoirs of Chang 8 Member is in the range of 0.1–36% (avg. 7.1%), showing no
260 significant trend with increasing burial depth (Figure 6C).

261 **4.3.4 Clay minerals**

262 Based on the XRD and SEM analysis, various types of clay minerals with different
263 amounts and textural habits are identified in the studied tight sandstone reservoirs.
264 The kaolinite, illite and chlorite are the most important types of authigenic clays. The
265 smectite and mixed-layer illite/smectite (I/S) are the minor clay minerals in the tight
266 sandstone of Chang 8 Member. These clay minerals are generally filling the primary
267 and secondary pores with different textural habits, for example, the kaolinite primarily
268 occurs as booklets and vermicular aggregates (Figure 8A, B), the smectite occurs as
269 curly flakes (Figure 8C), the mixed-layer illite/smectite (I/S) mainly occurs as foliated
270 or honeycomb aggregates (Figure 8D) and the illite occurs as fibrous and sometimes
271 honeycomb-textured masses (Figure 8E, F). In addition, the rosette-shaped and
272 needle-shaped chlorite occurs mainly as coatings and rims covering the framework
273 grain and authigenic quartz crystal (Figure 8 G-I). According the texture relationship,
274 two stages of chlorite are found in the studied tight sandstone reservoirs, the stage-I
275 chlorite formed before calcite and the stage-II chlorite formed after authigenic quartz.

276 In general, the kaolinite, illite, and chlorite in the tight sandstone reservoirs of
277 Chang 8 Member accounts for 1.4–51.2% (avg. 16.7%), 7–79% (avg. 34.6%) and
278 16.7–60.9% (avg. 45.2%) of the total clay content, respectively. In addition, the
279 kaolinite mainly exists at the depth shallower than about 2100 m, and reduces below
280 the depth (Figure 6D), where temperatures exceed to 110 °C. On of contrary, the
281 percentage of illite increases quickly at a depth deeper than about 2300 m, showing an
282 increase trend with increasing burial depth (Figure 6E). The content of chlorite
283 displays a slight increasing trend with the increasing burial depth (Figure 6F).

284 **4.4 Isotopic composition of carbonate cements**

285 59 tight sandstone samples were chosen for the isotopic composition analysis of

286 carbonate cements, and the details of all types and contents are summarized in Table 1.
287 Most calcite and dolomite have a relatively wide range of $\delta^{18}\text{O}$ values from -20.78‰
288 to -10.89‰ (avg. -15.11‰) and $\delta^{13}\text{C}$ from -10.23‰ to 1‰ (avg. -5.97‰).
289 Ferrocalcite and ankerite have a range of $\delta^{18}\text{O}$ values from -22.11‰ to -16.75‰ (avg.
290 -19.73‰) and $\delta^{13}\text{C}$ from -9.85‰ to -0.66‰ (avg. -4.96‰).

291 **4.5 Fluid inclusions**

292 The aqueous inclusions with a diameter about 2-12 μm , commonly present in the
293 quartz overgrowths, authigenic quartz crystals and carbonate cements in the tight
294 sandstone reservoirs of Chang 8 Member. Most of them are two-phase inclusions and
295 have gas bubbles at room temperature.

296 The measured homogenization temperatures (T_h) and final ice melting
297 temperature (T_m) of the aqueous inclusions in this study are shown in Table 2. Figure
298 9 presents the T_h distribution of aqueous inclusions in the quartz cements, including
299 overgrowths and authigenic quartz crystals. The formation temperature of carbonate
300 cements can be obtained both by the T_h of aqueous inclusions and the approximate
301 precipitation temperatures calculated by the oxygen isotope for all the studied samples
302 (Table 1). The aqueous inclusions in quartz overgrowths and authigenic quartz
303 crystals yield T_h ranges mainly from 77.3 °C to 123.5°C and from 71°C to 90°C,
304 respectively. The T_h of the aqueous inclusions in carbonate cements ranging mainly
305 from 51.7 °C to 117.8 °C. Meantime, the calculated precipitation temperatures for
306 the calcite/dolomite and the ferrocalcite/ankerite are in the range of 49.03–110.57 °C
307 and 79.93–140.32 °C, respectively.

308 **4.6 Pore water**

309 40 pore-water samples were measured from the tight sandstone reservoirs of Chang 8
310 Member. It indicated that approximately 73.3% characterized by CaCl_2 water, 13.3%
311 characterized by MgCl_2 water, 6.7% characterized by Na_2SO_4 water, and 6.7%
312 characterized by NaHCO_3 water. Generally, the salinity of pore water is high in these
313 samples, ranging from 3.2 g/L to 70.8 g/L. It shows an increasing trend with the burial

314 depth increasing, as well as the ion concentrations in the different solutes mentioned
315 above (Figure 10).

316 **5 DISCUSSION**

317 **5.1 Sources of carbonate cements**

318 Previous studies have suggested that there were three potential sources of carbonate
319 cements in the sandstone, including the external source (from adjacent mudstones or
320 source rocks, etc.), the internal source (e.g. locally reprecipitated detrital carbonate
321 grains or bioclasts), or a mixing of both (Dutton & Loucks, 2010; Gier et al., 2008). In
322 the tight sandstone reservoirs of Chang 8 Member, provenance evidences and
323 petrological feature show no occurrence of detrital carbonate grains and bioclasts,
324 indicating the carbonate cement should derive from the external source.

325 The $\delta^{13}\text{C}$ value of carbonate cements in the tight sandstone of Chang 8 Member
326 is in the range of $-10.2\text{--}1\text{‰}$, representing a single carbon source from the
327 decarboxylation of organic matter in the adjacent mudstone/source rocks (Figure 11A;
328 Irwin, Curtis, & Coleman, 1977). In addition, the $\delta^{13}\text{C}$ value increases with the
329 increasing distance of sample to the source rocks (Figure 11B), which indicating the
330 origin of carbonate cements were also controlled by the decarboxylation of organic
331 matter in the adjacent mudstones/source rocks (Xi et al., 2015a).

332 Previous studies have established that the ions of Ca^{2+} , Mg^{2+} and Fe^{2+} can be
333 provided by the conversion of volcanic rock fragments (Boles & Franks, 1979;
334 Stroker et al., 2013). As mentioned above, a large amount of unstable volcanic rock
335 fragments exists in the studied tight sandstone. In addition, the porosity of mudstones
336 in Chang 7 Member generally evolved from nearly 40% to mainly less than 10% at
337 present (Liu et al., 2012). During such a period, large amounts of advective
338 compaction fluids with Ca^{2+} , Mg^{2+} and Fe^{2+} were expelled from the mudstones to the
339 adjacent sandstones (Bjørlykke & Jahren, 2012; Xi et al., 2015a). As a result, the
340 concentrations of these ions are higher along the sandstone/mudstone interface than in
341 the central part of the sandstone body. When these ions mixed with the CO_3^{2-} which

342 derived from the organic matter decarboxylation in the adjacent mudstone, the initial
343 physical and chemical equilibrium is broken, allowing the carbonate to precipitate
344 (Dutton & Loucks, 2010; Milliken & Land, 1993). In this situation, the carbonate
345 cements preferentially concentrated in the marginal sandstone, showing a decrease
346 trend with the increasing distance to the sandstone/mudstone interface (Figure 12A).

347 **5.2 Sources of quartz and authigenic clay minerals**

348 In general, the concentrations of SiO_2 (aq) and Al^{3+} are extremely low in the pore
349 water of sandstone (Bjørlykke & Jahren, 2012, Xi et al., 2015a; Yuan et al., 2015a),
350 Due to the constraints of water volume and considerable heterogeneity in porosity and
351 permeability, the SiO_2 (aq) and Al^{3+} are difficult to transfer for a long distance from
352 the mudstone to the adjacent sandstone through advective flow, thermal convection or
353 diffusion, especially with the overlying mudstone of Chang 7 Member develops
354 overpressure (Bjørlykke & Jahren, 2012; Liu et al., 2012). However, the content of
355 quartz cements and authigenic clay minerals in the studied tight sandstone decreases
356 towards the sandstone/mudstone interface (Figure 12B, C), indicating that the quartz
357 cement and clay minerals in the tight sandstone reservoirs of Chang 8 Member should
358 originate from an internal source.

359 As the studied sandstones experienced the minimal dissolution pressure, it is
360 impossible that the quartz comes from the pressure dissolution. In addition, the
361 petrological observations from thin sections show that the quartz cements and
362 authigenic clays are always accompanied with feldspar dissolution pores (Figure 5I),
363 suggesting that the quartz cements and clay minerals are the byproducts of feldspar
364 dissolution. Furthermore, the positive relationship between the feldspar dissolution
365 porosity and content of clay/quartz cement (Figure 13A, B), also indicates that the
366 feldspar dissolution provides the source to quartz cements and authigenic clay
367 minerals, which is consistent with the results of previous studies (Giles & De Boer,
368 1990; Higgs et al., 2007; Yuan et al., 2015a).

369 **5.3 Diagenetic sequence**

370 Aqueous inclusions can provide valuable information for the precipitation
371 temperature of authigenic minerals (Robinson & Gluyas, 1992). In this study, the
372 homogenization temperatures (T_h) of fluid inclusions (including the precipitation
373 temperatures calculating by oxygen isotope values of carbonate cements, and the T_h of
374 fluid inclusions in quartz and carbonate cements) and texture relationship can be used
375 to infer the relative timing of major diagenetic sequence and reconstruct the
376 diagenetic history of the tight sandstone reservoirs in Chang 8 Member.

377 The T_h of aqueous inclusions ranges from 71°C to 123.5°C in the quartz
378 cements with an average of 97.4°C, and from 41.03°C to 140.32°C in the carbonate
379 cements. However, two T_h peaks of aqueous inclusions have been observed in the
380 carbonate cements, mainly ranging from 50°C to 70°C and 100°C to 130°C (Figure
381 9), which suggests that there are two stages of carbonate cementation. The dolomite
382 cements were always replaced by the ferrocalcite and ankerite, and the ferrocalcite
383 and ankerite cements mainly filled in the pores around the euhedral authigenic quartz
384 crystal (Figure 7E-H). It indicates that the dolomite and quartz cements formed before
385 the ferrocalcite and ankerite cements. Therefore, the two T_h peaks of carbonate
386 cements are respectively correspond to the T_h of calcite/dolomite and
387 ferrocalcite/ankerite. In addition, the calcite mainly cemented the point-linear contact
388 grains (Figure 7A, 8H), indicating an early stage of diagenesis when cementation
389 occurred. Moreover, there is no authigenic quartz replaced by calcite/dolomite cement.
390 As a result, based on the T_h of fluid inclusions in carbonate and quartz cements, it is
391 inferred that the authigenic quartz cement formed later than the early carbonate
392 cement (calcite/dolomite) and earlier than the late carbonate cement
393 (ferrocalcite/ankerite).

394 As a whole, with the constraints of petrographic evidences described above
395 (Figure 5, 7, 8), the source analysis of related diagenetic minerals, and the
396 burial-thermal history of well Xi17 in Xifeng Area, the diagenetic sequence of Chang
397 8 Member tight sandstone can be summarized in Figure 14.

398 **5.4 Types of diagenetic geochemical system**

399 The salinity of pore water shows an increase trend with the burial depth increases
400 (Figure 10), suggesting limited advective mixing of pore waters from different origins
401 (Bjørlykke & Gran, 1994; Bjørlykke & Jahren, 2012). Since the studied sandstone
402 escaped the near-surface water quickly with rapid burial (Figure 14), it indicates little
403 impact of meteoric water after deposition. The overlying Chang 7 Member commonly
404 developed moderate to strong fluid overpressure with few faults, which can strongly
405 reduce the penetration of meteoric water in Chang 8 Member (Liu et al., 2012). It is
406 consistent with the result that there is little impact of meteoric water due to the
407 overlying overpressure (Bjørlykke, 1993; Yuan et al., 2015b). Moreover, a large
408 number of authigenic illite formed when burial depth was greater than 2300m (Figure
409 6D), at the moment the temperature was about 120°C (Figure 14). In such a situation,
410 the concentration of K⁺ in the pore water from Chang 8 Member tight sandstone is in
411 the range of 0.019–1.1g/L (Figure 10), most of which were greater than 0.12g/L (the
412 minimum concentration of K⁺ for illitization when the temperature >120 °C)
413 (Bjørlykke, 1998). Thus, the concentration of K⁺ can promote the illitization of
414 kaolinite and K-feldspar. Therefore, it can be concluded that enough K⁺ should have
415 retained in the studied tight sandstone systems because of the occurrence of illitization
416 reactions, which indicates a closed geochemical system during the diagenesis.

417 In addition, the salinity of pore water during the diagenesis can be calculated by
418 the ice melting temperature (T_m) of aqueous fluid inclusions in the quartz cements and
419 carbonate cements (Table 2). It is in the range of 3.55–20.67%, mostly greater than
420 10%, showing an increasing trend with the burial depth increasing (Figure 15).
421 Moreover, the contents of carbonate cements, quartz cements, authigenic clay
422 minerals and feldspar dissolution pores show slightly variation within the sandstone
423 when the distance to the sandstone/mudstone interface more than 1m (Figure 12 A-D).
424 These above phenomena all indicated that there is less mass transfer between the
425 internal and external environment during the diagenesis. Thus, it can be concluded
426 that the tight sandstone of Chang 8 Member should be in a closed geochemical system.

427 Furthermore, from the petrological evidences, the authigenic quartz and clay minerals,
428 as the byproducts always accompanied with feldspar dissolution, without
429 long-distance transportation. It is also consistent with a closed geochemical system.
430 Therefore, combining the analysis of petrographic texture relationship, distribution
431 pattern of authigenic minerals and feldspar dissolution, characteristics of pore water,
432 salinity of diagenetic fluid and geologic setting of Xifeng Area, it suggests that the
433 geochemical system is closed during the diagenesis of Chang 8 Member tight
434 sandstone reservoir.

435 **5.5 Effects of diagenetic geochemical system on tight sandstone reservoir quality**

436 As the tight sandstone reservoirs of Chang 8 Member were in a closed geochemical
437 system during the diagenesis, the diagenetic mass could not effectively transport in
438 the pore water to exchange with the external materials (Bjørlykke & Jahren, 2012).
439 Thus, the diagenetic reactions including mineral dissolution and precipitation always
440 occur in a confined space, in where the authigenic quartz and clay minerals cements
441 result from feldspar dissolution are always exist together with the dissolution pores
442 within the studied tight sandstone (Figure 5I). Generally, the feldspar dissolution
443 could improve the reservoir quality, however, the cementation of quartz and clay
444 minerals have a negative impact on the porosity and permeability of tight sandstone.
445 In addition, due to the closed diagenetic system, the carbonate cements preferentially
446 concentrated in the marginal sandstones (distance to the sandstone/mudstone interface
447 mainly less than 1 m), preventing the external pore water with CO_3^{2-} ion from flowing
448 to the central sandstone (Figure 12A).

449 In order to analyze the diagenetic process of feldspar dissolution and how its
450 precipitated byproducts simultaneously affect the sandstone porosity, the content of
451 feldspar dissolution pores, clay and quartz cement can be evaluated in the thin
452 sections (Yuan et al., 2015b). The difference value between the feldspar dissolution
453 porosity and the sum of byproducts in Chang 8 Member is in the range of -1.07–1.03%
454 (avg. 0.07%) (Figure 16), which means the minerals alternation has little impact on
455 the absolute porosity of sandstone reservoir in the diagenetic process under a closed

456 system. Besides, the porosity of core samples shows an insignificant trend with the
457 increasing feldspar dissolution porosity (Figure 17A). Although the feldspar
458 dissolution releases some pore space, its byproducts occupy some primary
459 intergranular pore as well, which means the pore space is just redistributed from the
460 primary intergranular pores converting to the feldspar dissolution pores and clay
461 minerals micropores (Giles & De Boer, 1990; Yuan et al., 2015b). Meantime, the
462 permeability of the studied tight sandstone shows a decreasing trend with the
463 proportion of dissolved feldspar increasing (Figure 17B). It suggested that the clays
464 derived from feldspar dissolution blocked the pores and pore throats in the tight
465 sandstone that resulted in a significant decrease in permeability.

466 As a whole, the porosity and permeability of the studied tight sandstone are
467 controlled by the closed geochemical system during diagenesis. In general, the
468 porosity and permeability increase with the increasing distance to the sandstone/
469 mudstone interface, especially when the distance is more than 1 m (Figure 12E, F).
470 Therefore, the reservoirs in the tight sandstone of Chang 8 Member mainly develop in
471 the central part of the sandstone. Tight sandstone with thickness more than 2 m could
472 be the potential hydrocarbon reservoirs.

473 **5.6 Implications**

474 As mentioned before, previous studies suggested the reservoir quality of tight
475 sandstone was affected by the diagenesis just based on the descriptions of diagenetic
476 characteristics (Higgs et al., 2007; Lai, Wang, Ran, Zhou, & Cui, 2016; Stroker et al.,
477 2013; Wang et al., 2017; Xi et al., 2015a; Zhou et al., 2016). Although the
478 relationships between diagenesis and reservoir quality have been discussed
479 systematically in most research areas, the essential cause of the tight sandstone
480 reservoir with high porosity remains a puzzle.

481 Essentially, the origin, transfer, dissolution and precipitation of diagenetic
482 minerals are caused by the water-rock interactions, which were controlled by the
483 diagenetic geochemical system (Bjørlykke & Jahren, 2012). This study discusses the
484 diagenesis which is constrained in the diagenetic geochemical system, and

485 demonstrates how the precipitation, dissolution and reprecipitation of diagenetic
486 minerals were controlled by the diagenetic geochemical system. Here a combination
487 of the sandstones and adjacent mudstones in Chang 8 Member constitutes a complete
488 and closed system. Although the specific minerals differ, a similar conclusion was
489 concluded by analyzing the diagenesis within the Upper Jurassic Brae Formation of
490 the North Sea, in which solutes were supplied from the mudstones into adjacent
491 sandstones and the average porosity of sandstone displayed a positive correlation with
492 both bed thickness and net to gross (Gluyas, Garland, Oxtoby, & Hogg, 2000).

493 Due to the relatively closed diagenetic system, the diagenetic fluids could not
494 effectively exchange with the external fluids. Thus, the external sourced carbonate
495 cements mainly develop in the marginal sandstone and could not develop into the
496 central sandstone. In addition, the diagenetic fluids with SiO_2 (aq), Al^{3+} and K^+ are
497 difficult to transfer for a long distance between the mudstone and the adjacent
498 sandstone. As a result, the byproducts of feldspar dissolution including quartz and
499 clay minerals just generate in the central sandstone. The pore space of the central
500 sandstone is preserved and only redistributed. Therefore, the sweet zones in the
501 sandstone reservoirs dominantly develop in the central sandstone. Thus, the reservoir
502 quality of tight oil sandstone is essentially controlled by the diagenetic system. In fact,
503 the diagenetic system can be used for explaining some similar diagenetic
504 characteristics observed in tight sandstone over the world. For example, the carbonate
505 cements commonly concentrated along the sandstone/mudstone interface in Yanchang
506 Formation of Longdong area and Zhenjing area, Ordos Basin and Quantou Formation
507 of southern Songliao Basin, China (Wang et al., 2017; Xi et al., 2015a; Zhou et al.,
508 2016). Moreover, the reaction of feldspar dissolution accompanied with precipitation
509 of authigenic quartz and clays in Quantou Formation of southern Songliao Basin,
510 China and the K3E Kapuni Group in Taranaki Basin, New Zealand (Xi et al., 2015a;
511 Higgs et al., 2007). There is an approximate balance between decrease of primary
512 porosity and increase of secondary porosity in the Upper Cretaceous Mesaverde
513 sandstones of the Piceance Basin, western Colorado (Stroker, et al., 2013). Based on
514 the analysis of this study, it can be concluded that the diagenesis of the above tight

515 sandstone occurred in a closed diagenetic system. In addition, the dissolution pores
516 developed around the faults in Carboniferous tight sandstone of the Lower Saxony
517 Basin, Northern Germany, suggesting the leaching of acidic fluid in an open
518 diagenetic system (Wüstefeld, Hilse, Koehrer, Adelman, & Hilgers, 2017). Although
519 detailed clues of diagenetic processes have been given to reveal the intrinsic relation
520 of diagenesis, a comprehensive diagenetic system has been ignored by analyzing
521 diagenesis separately. As a result, the most essential diagenetic process and reservoir
522 heterogeneity of tight sandstone cannot be fully understood. Therefore, the theory of
523 the diagenetic geochemical system should be applied in the study of tight sandstone
524 diagenesis.

525 That the pattern of diagenetic geochemical system controlling the quality of tight
526 oil sandstone provides a useful analogue for understanding the quality evolution of the
527 tight oil sandstone reservoir which experienced complicated diagenesis. It will be
528 useful for predict the potential reservoirs in other tight sandstones worldwide.

529 **6 CONCLUSIONS**

- 530 1. The tight sandstone of Chang 8 Member in Xifeng Area are mostly lithic arkoses
531 and feldspathic litharenites with low porosity (mainly 4% to 16%) and permeability
532 (mostly <1mD). And it has undergone significant chemical diagenesis including
533 precipitation of quartz, clay minerals (mainly kaolinite, illite and chlorite) and
534 carbonate (mainly calcite, dolomite, ferrocalcite and ankerite) and dissolution of
535 feldspar.
- 536 2. The petrographic textural relationships, the distribution pattern of authigenic
537 minerals and feldspar dissolution, the characteristics of pore water, the salinity of
538 diagenetic fluid and the geologic setting of Xifeng Area, all indicate that the
539 geochemical system was closed during diagenesis period of the tight sandstone
540 reservoir in Chang 8 Member.
- 541 3. The relatively closed diagenetic geochemical system impacts the main chemical
542 diagenetic alterations. The carbonate cements preferentially concentrated in the

543 marginal sandstone (distance to the sandstone/mudstone interface mainly less than
544 1 m) that result from interaction of the sandstones with carbon (as carbonate)
545 sourced from the adjacent mudstones. The cements of quartz and clay minerals are
546 the byproducts of feldspar dissolution and always associate with feldspar
547 dissolution pores due to internal sources of quartz and clay minerals affected by the
548 closed system.

549 4. The reservoir quality of the marginal sandstone is poor due to the carbonate
550 cementation, and this effect typically extends no more than 1m from the sandstone
551 margin. Therefore, the reservoirs in the tight sandstone mainly develop in the
552 central part. Tight sandstone with thickness more than 2 m could be the potential
553 hydrocarbon reservoirs.

554 5. The pattern of diagenetic geochemical system controls the quality of tight oil
555 sandstone, which can provide guidance for predicting the high-quality reservoirs in
556 other tight sandstones worldwide.

557 **ACKNOWLEDGEMENTS**

558 This study was financially supported by the Natural Science Foundation of China
559 (Grant No. 41502147, Grant No. 41672124), Project funded by China Postdoctoral
560 Science Foundation (Grant No. 2016M600752), Sichuan Province Education
561 Department Foundation (Grant No. 16ZA0072) and National science and technology
562 major project of China (2016ZX05047001-002). The PetroChina Research Institute of
563 Petroleum Exploration & Development and PetroChina Changqing Oilfield Company
564 are thanked for providing basic data. Special thanks are extended to the editors and
565 anonymous reviewers for their detailed and constructive suggestions.

566 **REFERENCES**

567 Bjørlykke, K. (1993). Fluid flow in sedimentary basins. *Sedimentary Geology*, 86,
568 137-158.

569 Bjørlykke, K. (1998). Clay mineral diagenesis in sedimentary basins-A key to the

570 prediction of rock properties. Examples from the North Sea Basin. *Clay Minerals*,
571 33, 15-34.

572 Bjørlykke, K., & Gran, K. (1994). Salinity variations in North Sea formation waters:
573 Implications for large-scale fluid movements. *Marine and Petroleum Geology*,
574 11, 5-9.

575 Bjørlykke, K., & Jahren, J. (2012). Open or closed geochemical systems during
576 diagenesis in sedimentary basins: constraints on mass transfer during diagenesis
577 and the prediction of porosity in sandstone and carbonate reservoirs. *AAPG*
578 *Bulletin*, 96, 2193-2214.

579 Bodnar, R.J. (1993). Revised equation and table for determining the freezing point
580 depression of H₂O-NaCl solutions. *Geochimica et Cosmochimica Acta*, 57,
581 683-684.

582 Boles, J.R., & Franks, S.G. (1979). Clay diagenesis in Wilcox sandstones of
583 southwest Texas: implications of smectite diagenesis on sandstone cementation.
584 *Journal of Sedimentary Research*, 49, 55-70.

585 Chuhan, F. A., Bjørlykke, K., & Lowrey, C. (2001). Closed system burial diagenesis
586 in reservoir sandstones: Examples from the Garn Formation at Haltenbanken
587 area, offshore mid-Norway. *Journal of Sedimentary Research*, 71, 15-26.

588 Coplen, T. B., Kendall, C., & Hopple, J. (1983). Comparison of stable isotope
589 reference samples. *Nature*, 302, 236-238.

590 Cui, Y. F., Wang, G. W., Jones, S. J., Zhou, Z. L., Ran, Y., Lai, J., LI, R. J., & Deng, L.
591 (2017). Prediction of diagenetic facies using well logs -A case study from the
592 upper Triassic Yanchang Formation, Ordos Basin, China. *Marine and Petroleum*
593 *Geology*, 81, 50-65.

594 Day-Stirrat, R. J., Milliken, K. L., Dutton, S. P., Loucks, R. G., Hillier, S., Aplin, A.
595 C., & Schleicher, A. M. (2010). Open-system chemical behavior in deep Wilcox
596 Group mudstones, Texas Gulf Coast, USA. *Marine and Petroleum Geology*, 27,
597 1804-1818.

598 Dou, W. C., Liu, L. F., Wu, K. J., Xu, Z. J., & Feng, X. (2017). Origin and
599 significance of secondary porosity: A case study of upper Triassic tight

600 sandstones of Yanchang Formation in Ordos basin, China. *Journal of Petroleum*
601 *Science and Engineering*, 149, 485-496.

602 Dutton, S. P., & Loucks, R.G. (2010). Diagenetic controls on evolution of porosity
603 and permeability in lower Tertiary Wilcox sandstones from shallow to ultradeep
604 (200-6700m) burial, Gulf of Mexico Basin, U.S.A. *Marine and Petroleum*
605 *Geology*, 27, 69-81.

606 Ehrenberg, S.N. (1990). Relationship between diagenesis and reservoir quality in
607 sandstones of the Garn formation, Haltenbanken, mid-norwegian continental
608 shelf. *AAPG Bulletin*, 74, 1538-1558.

609 Friedman, I., & O'Neil, J.R. (1977). Compilation of Stable Isotope Fractionation
610 Factors of Geochemical Interest, in Data of Geochemistry. *US Government*
611 *Printing Office*, 440.

612 Folk, R.L., 1974. Petrology of Sedimentary Rocks. *Hemphill*, 182.

613 Fu, J. H., Deng, X. Q., Wang, Q., Li, J.H., Qiu, J. L., Hao, L. W., & Zhao, Y. D.
614 (2017). Densification and hydrocarbon accumulation of Triassic Yanchang
615 Formation Chang 8 Member, Ordos Basin, NW China: Evidence from
616 geochemistry and fluid inclusions. *Petroleum Exploration and Development*, 44,
617 48-57.

618 Gier, S., Worden, R. H., Jones, W. D., & Kurzweil, H. (2008). Diagenesis and
619 reservoir quality of Miocene sandstones in the Vienna Basin, Australia. *Marine*
620 *and Petroleum Geology*, 25, 681-695.

621 Giles, M.R., & De Boer, R.B. (1990). Origin and significance of redistributive
622 secondary porosity. *Marine and Petroleum Geology*, 7, 378-397.

623 Gluyas, J., & Coleman, M. L. (1992). Material flux and porosity changes during
624 sediment diagenesis. *Nature*, 356, 52-53.

625 Gluyas, J., Garland, C., Oxtoby, N. H., & Hogg, A. J. C. (2000). Quartz cement: the
626 Miller's tale. *Quartz cementation in sandstones*, 29,199-218.

627 Guo, Y. R., Liu, J. B., Yang, H., Liu, Z., Fu, J. H., Yao, J. L., Xu, W. L., & Zhang, Y. L.
628 (2012). Hydrocarbon accumulation mechanism of low permeable tight lithologic
629 oil fields in the Yanchang Formation, Ordos Basin, China. *Petroleum*

630 *Exploration and Development*, 39, 447-456.

631 He, Z. X. (2003). *Evolution and hydrocarbon resource of the Ordos Basin*. Petroleum
632 Industry Press. Beijing (in Chinese with English abstract).

633 Higgs, K. E., Zwingmann, H., Reyes, A. G., & Funnell, R. H. (2007). Diagenesis,
634 porosity evolution, and petroleum emplacement in tight gas reservoirs, Taranaki
635 Basin, New Zealand. *Journal of Sedimentary Research*, 77, 1003-1025.

636 Irwin, H., Curtis, C., & Coleman, M. (1977). Isotopic evidence for source of
637 diagenetic carbonates formed during burial of organic-rich sediments. *Nature*,
638 269, 209-213.

639 Law, B. E., & Curtis, J. B. (2002). Introduction to unconventional petroleum systems.
640 *AAPG Bulletin*, 86, 1851-1852.

641 Lai, J., Wang, G., Ran, Y., Zhou, Z., & Cui, Y. (2016). Impact of diagenesis on the
642 reservoir quality of tight oil sandstones: the case of Upper Triassic Yanchang
643 Formation Chang 7 oil layers in Ordos Basin, China. *Journal of Petroleum
644 Science and Engineering*, 145, 54-65.

645 Liu, M. J., Liu, Z., Liu, J. J., Zhu, W. Q., Huang, Y. H., & Yao, X. (2014). Coupling
646 relationship between sandstone reservoir densification and hydrocarbon
647 accumulation: A case from the Yanchang Formation of the Xifeng and Ansai
648 areas, Ordos Basin. *Petroleum Exploration and Development*, 41, 185 -192.

649 Liu, M. J., Liu, Z., Wang, P., & Pan, G. F. (2016). Diagenesis of the Triassic Yanchang
650 Formation Tight Sandstone Reservoir in the Xifeng-Ansai Area of Ordos Basin
651 and its Porosity Evolution. *Acta Geologica Sinica (English Edition)*, 90,
652 956-970.

653 Liu, M. J., Liu, Z., Wu, Y. W., Zhu, W. Q., & Wang, P. (2017). Differences in
654 formation process of tight sandstone gas reservoirs in different substructures in
655 Changling Fault Depression, Songliao Basin, NE China. *Petroleum Exploration
656 and Development*, 44, 257-264.

657 Liu, Q. S., Chan, L. S., Liu, Q. S., Li, H. X., Wang, F., Zhang, S. X., Xia, X. H., &
658 Cheng, T. J. (2004). Relationship between magnetic anomalies and hydrocarbon
659 microseepage above the Jingbian gas field, Ordos basin, China. *AAPG Bulletin*,

660 88, 241-251.

661 Liu, Z., Chen, K., Zhu, W. Q., Hu, X. D., Guo, Y. R., & Wu, X. D. (2012).
662 Paleo-pressure restoration of Chang 7 shale in Xifeng area, Ordos Basin. *Journal*
663 *of China University Petroleum (Edition of Natural Sciences)*, 36, 1-7 (in Chinese
664 with English abstract).

665 Liu, Z., Zhu, W. Q., Xia, L., Pan, G. F., Wu, X. D., & Guo, Y. R. (2013). Research on
666 oil accumulation process of lithologic reservoir in Chang 8 Member of Yanchang
667 Formation, Xifeng Oilfield. *Geoscience*, 27, 895-906 (in Chinese with English
668 abstract).

669 Maast, T. E., Jahren, J., & Bjørlykke, K. (2011). Diagenetic controls on reservoir
670 quality in Middle to Upper Jurassic sandstones in the South Viking Graben,
671 North Sea. *AAPG Bulletin*, 95, 1937 - 1958.

672 Mansurberg, H., Caja, M. A., Marfil, R., Morad, S., Remacha, E., Martin-Crespo, T.,
673 El-Ghali, M.A.K., & Nystuen, J.P. (2009). Diagenetic evolution and porosity
674 destruction of turbiditic hybrid arenites and siliciclastic sandstones of foreland
675 basin: evidence from the Eocene Hecho Group, Pyrenees, Spain. *Journal of*
676 *Sedimentary Research*, 79, 711-735.

677 Matthews, A., & Katz, A. (1977). Oxygen isotope fractionation during the
678 dolomitization of calcium carbonate. *Geochimica et Cosmochimica Acta*, 41,
679 1431-1438.

680 Milliken, K.L., & Land, L.S. (1993). The origin and fate of silt sized carbonate in
681 subsurface Miocene-Oligocene mudstones, south Texas Gulf Coast.
682 *Sedimentology*, 40, 107-124.

683 Morad, S., Ketzer, J.M., & DeRos, L.F. (2000). Spatial and temporal distribution of
684 diagenetic alterations in siliciclastic rocks: implications for mass transfer in
685 sedimentary basins. *Sedimentology*, 46, 95-120.

686 Qiu, X., Liu, C., Wang, F., Deng, Y., & Mao, G. (2015). Trace and rare earth element
687 geochemistry of the upper Triassic mudstones in the southern Ordos Basin,
688 Central China. *Geological Journal*, 50, 399- 413.

689 Ren, Z.L., Zhang, S., Gao, S.L., Cui, J. P., Xiao, Y. Y., & Xiao, H. (2007). Tectonic

690 thermal history and its significance on the formation of oil and gas accumulation
691 and mineral deposit in Ordos Basin. *Science in China Series D: Earth Sciences*,
692 37, 23–32.

693 Robinson, A., & Gluyas, J. (1992). Duration of quartz cementation in sandstones,
694 North Sea and Haltenbanken Basins. *Marine and Petroleum Geology*, 9,
695 324-327.

696 Schmitt, M., Fernandes, C. P., Wolf, F. G., da Cunha Neto, J. A. B., Rahner, C. P., &
697 dos Santos, V. S. S. (2015). Characterization of Brazilian tight gas sandstones
698 relating permeability and Angstrom-to micron-scale pore structures. *Journal of*
699 *Natural Gas Science and Engineering*, 27, 785-807.

700 Spencer, C. W. (1985). Geologic aspects of tight gas reservoirs in the Rocky Mountain
701 region. *Journal of Petroleum Technology*, 37,1308-1314.

702 Stroker, T.M., Harris, N.B., Crawford Elliott, W., & Marion Wampler, J. (2013).
703 Diagenesis of a tight gas sand reservoir: Upper Cretaceous Mesaverde Group,
704 Piceance Basin, Colorado. *Marine and Petroleum Geology*, 40, 48-68.

705 Taylor, T. R., Giles, M. R., Hathon, L. A., Diggs, T. N., Braunsdorf, N. F., Birbigilia,
706 G. V., Kittridge, M.G., Macaulay, C. I., & Espejo, I. S. (2010). Sandstone
707 diagenesis and reservoir quality prediction: Models, myths, and reality. *AAPG*
708 *Bulletin*, 94, 1093-1132.

709 Umar, M., Friis, H., Khan, A. S., Kassi, A. M., & Kasi, A. K. (2011). The effects of
710 diagenesis on the reservoir characters in sandstones of the Late Cretaceous Pab
711 Formation, Kirthar Fold Belt, southern Pakistan. *Journal of Asian Earth Sciences*,
712 40, 622-635.

713 Wang, G. W., Chang, X. C., Yin, W., Li, Y., & Song, T. T. (2017). Impact of
714 diagenesis on reservoir quality and heterogeneity of the Upper Triassic Chang 8
715 tight oil sandstones in the Zhenjing area, Ordos Basin, China. *Marine and*
716 *Petroleum Geology*, 83, 84-96.

717 Wu, S. T., Zou, C. N., Zhu, R. K., Yao, J. L., Tao, S. Z., Yang, Z., Zhai, X. F., Cui, J.
718 W., & Lin, S. H. (2016). Characteristics and origin of tight oil accumulations in
719 the Upper Triassic Yanchang Formation of the Ordos Basin, North-Central China.

720 *Acta Geologica Sinica (English Edition)*, 90, 1821-1837.

721 Wüstefeld, P., Hilse, U., Koehrer, B., Adelman, D., & Hilgers, C. (2017). Critical
722 evaluation of an Upper Carboniferous tight gas sandstone reservoir analog:
723 Diagenesis and petrophysical aspects. *Marine and Petroleum Geology*, 86,
724 689-710.

725 Xi, K. L., Cao, Y. C., Jaren, J., Zhu, R. K., Bjørlykke, K., Haile, B. G., Zheng, L. J.,
726 & Hellevang, H. (2015a). Diagenesis and reservoir quality of the Lower
727 Cretaceous Quantou Formation tight sandstones in the southern Songliao Basin,
728 China. *Sedimentary Geology*, 330, 90-107.

729 Xi, K. L., Cao, Y. C., Jaren, J., Zhu, R. K., Bjørlykke, K., Zhang, X. X., Cai, L. X., &
730 Hellevang, H. (2015b). Quartz cement and its origin in tight sandstone reservoirs
731 of the Cretaceous Quantou Formation in the southern Songliao Basin, China.
732 *Marine and Petroleum Geology*, 66, 748-763.

733 Xu, Z. J., Liu, L. F., Wang, T. G., Wu, K. J., Gao, X. Y., Dou, W. C., Xiao, F., Zhang,
734 N. N., Song, X. P., & Ji, H. T. (2017). Application of fluid inclusions to the
735 charging process of the lacustrine tight oil reservoir in the Triassic Yanchang
736 Formation in the Ordos Basin, China. *Journal of Petroleum Science and*
737 *Engineering*, 149, 40-45.

738 Yang, H., Li, S.X., & Liu, X.Y. (2013). Characteristics and resource prospects of tight
739 oil and shale oil in Ordos Basin. *Acta Petrolei Sinica*, 34, 1-11 (in Chinese with
740 English abstract).

741 Yang, H., Liu, X.Y., Zhang, C.L., Han, T.Y., & Hui, X. (2007). The main controlling
742 factors and distribution of low permeability lithologic reservoirs of Triassic
743 Yanchang Formation in Ordos Basin. *Lithologic Reservoirs*, 19, 1-6 (in Chinese
744 with English abstract).

745 Yang, H., & Zhang, W.Z. (2005). Leading effect of the seventh Member high-quality
746 source rock of Yanchang Formation in Ordos Basin during the enrichment of
747 low-penetrating oil-gas accumulation: geology and geochemistry. *Geochimica*,
748 34, 147-154 (in Chinese with English abstract).

749 Yang, J. J. (2002). *Tectonic evolution and oil-gas reservoirs distribution in Ordos*

750 *Basin. Petroleum Industry Press. Beijing (in Chinese with English abstract).*

751 Yang, R. C., Jin, Z., J., Van Loon, A., J., Han, Z., Z., & Fan, A., P. (2017). Climatic
752 and tectonic controls of lacustrine hyperpycnite origination in the Late Triassic
753 Ordos Basin, central China: Implications for unconventional petroleum
754 development. *AAPG Bulletin*, 101, 95-117.

755 Yao, J.L., Deng, X.Q., Zhao, Y.D., Han, T.Y., Chu, M.J., & Pang, X.L. (2013).
756 Characteristics of tight oil in Triassic Yanchang formation, Ordos basin.
757 *Petroleum Exploration and Development*, 40, 161-169.

758 Yuan, G.H., Cao, Y.C., Gluyas, J., Li, X.Y., Xi, K.L., Wang, Y.Z., Jia, Z.Z., Sun, P.P.,
759 & Oxtoby, N.H. (2015b). Feldspar dissolution, authigenic clays, and quartz
760 cements in open and closed sandstone geochemical systems during diagenesis:
761 typical examples from two sags in Bohai Bay Basin, East China. *AAPG Bulletin*,
762 99, 2121-2154.

763 Yuan, G.H., Cao, Y.C., Zhang, Y. C., & Gluyas, J. (2017). Diagenesis and reservoir
764 quality of sandstones with ancient “deep” incursion of meteoric freshwaterddAn
765 example in the Nanpu Sag, Bohai Bay Basin, East China. *Marine and Petroleum*
766 *Geology*, 82, 444-464.

767 Yuan, G. H., Gluyas, J., Cao, Y. C., Oxtoby, N. H., Jia, Z. Z., Wang, Y. Z., Xi, K. L., &
768 Li, X. Y. (2015a). Diagenesis and reservoir quality evolution of the Eocene
769 sandstones in the northern Dongying Sag, Bohai Bay Basin, East China. *Marine*
770 *and Petroleum Geology*, 62, 77-89.

771 Zhang, W.Z., Yang, H., Li, J. F., & Ma, J. (2006). Leading effect of high class source
772 rock of Chang 7 in Ordos Basin on enrichment of low permeability oil-gas
773 accumulation: Hydrocarbon generation and expulsion mechanism. *Petroleum*
774 *Exploration and Development*, 33, 289-293 (in Chinese with English abstract).

775 Zhang, W.Z., Yang, H., Hou, L.H., & Liu, F. (2009). Distribution and geological
776 significance of 17 α (H)-diahopanes from different hydrocarbon source rocks of
777 Yanchang Formation in Ordos Basin. *Science in China Series D: Earth Sciences*,
778 52, 965-974.

779 Zhang, Y., Pe-piper, G., & Piper, D. J.W. (2015). How sandstone porosity and

780 permeability vary with diagenetic minerals in the Scotian Basin, offshore eastern
781 Canada: Implications for reservoir quality. *Marine and Petroleum Geology*, 63,
782 28-45.

783 Zhang, Y. L., Bao, Z. D., Zhao, Y., Jiang, L., & Gong, F. H. (2017). Diagenesis and its
784 controls on reservoir properties and hydrocarbon potential in tight sandstone: a
785 case study from the Upper Triassic Chang 7 oil group of Yanchang Formation,
786 Ordos Basin, China. *Arabian Journal of Geosciences*, 10, 234.

787 Zhou, Y., Ji, Y. L., Xu, L. M., Che, S. Q., Niu, X. B., Wan, L., Zhou, Y. Q., Li, Z. C.,
788 & You, Y. (2016). Controls on reservoir heterogeneity of tight sand oil reservoirs
789 in Upper Triassic Yanchang Formation in Longdong Area, southwest Ordos
790 Basin, China: Implications for reservoir quality prediction and oil accumulation.
791 *Marine and Petroleum Geology*, 78, 110-135.

792 Zhu, H. H., Zhong, D.K., Yao, J.L., Sun, H.T., Niu, X.B., Liang, X.W., You, Y., & Li,
793 X. (2015).
794 Alkaline diagenesis and its effects on reservoir porosity: a case study of Upper
795 Triassic Chang7 Member tight sandstone in Ordos Basin, NW China. *Petroleum*
796 *Exploration and Development*, 42, 56-65.

797 Zou, C. N., Wang, L., Li, Y., Tao, S. Z., & Hou, L. H. (2012b). Deep-lacustrine
798 transformation of sandy debrites into turbidites, Upper Triassic, Central China.
799 *Sedimentary Geology*, 265, 143-155.

800 Zou, C.N., Zhang, G.Y., Tao, S.Z., Hu, S.Y., Li, X.D., Li, J.Z., Dong, D.Z., Zhu, R.K.,
801 Yuan, X.J., Hou, L.H., Qu, H., Zhao, X., Jia, J.H., Gao, X.H., Guo, Q.L., Wang,
802 L., & Li, X.J. (2010a). Geological features, major discoveries and
803 unconventional petroleum geology in the global petroleum exploration.
804 *Petroleum Exploration and Development*, 37, 129-145.

805 Zou, C.N., Zhang, X. Y., Luo, P., Wang, L., Luo, Z., & Liu, L. H. (2010b).
806 Shallow-lacustrine sand-rich deltaic depositional cycles and sequence
807 stratigraphy of the Upper Triassic Yanchang Formation, Ordos Basin, China.
808 *Basin Research*, 22, 108-125.

809 Zou, C.N., Zhu, R.K., Liu, K., Su, L., Bai, B., & Zhang, X. (2012a). Tight gas

810 sandstone reservoirs in China: characteristics and recognition criteria. *Journal of*
811 *Petroleum Science and Engineering*, 88, 82-91.

812

Table 1

813

Mineralogical and isotopic composition of carbonate cements, and calculated formation temperature of cements in Chang 8

814

member tight sandstones of Xifeng Area. Ca-calcite, Do-dolomite, Fc-ferrocalcite, An-ankerite

Well	Depth, m	Carbonate mineral	$\delta^{13}\text{C}_{\text{PDB}}$ ‰	$\delta^{18}\text{O}_{\text{PDB}}$ ‰	Temperature, °C $\delta^{18}\text{O}_{\text{SMOW}}$ =-7‰	Well	Depth, m	Carbonate mineral	$\delta^{13}\text{C}_{\text{PDB}}$ ‰	$\delta^{18}\text{O}_{\text{PDB}}$ ‰	Temperature, °C $\delta^{18}\text{O}_{\text{SMOW}}$ w=-7‰
Wu121	2070.3	100% An	-2.18	-18.47	103.70	Xi200	2202.5	100% An	-5.35	-18.72	105.95
Wu121	2083.5	75% An+15% Ca+10% Do	-3.48	-20.10	118.88	Xi203	1873.6	100% An	-3.69	-18.71	105.83
Wu121	2076.8	100% An	-6.42	-20.12	119.00	Xi211	1580.5	100% An	-6.49	-17.59	96.28
Wu121	2081.55	100% Fc	-1.39	-17.36	79.93	Xi211	1548.1	95% Ca+5% Do	1.00	-12.88	49.03
Wu121	2082.45	90% Fc+10% An	-6.14	-19.32	96.53	Xi220	1944.9	100% An	-3.98	-19.87	116.65
Wu121	2093.9	100% Fc	-3.32	-20.15	104.30	Xi23	2095	100% An	-7.44	-16.75	89.51
Wu121	2090.5	100% Fc	-5.68	-19.98	102.68	Xi23	2090.7	100% An	-5.58	-18.04	100.05
Wu121	2087.9	100% Fc	-2.21	-19.59	98.98	Xi32	1940	100% An	-4.48	-19.50	113.11
Wu121	2081	90% Do+10% Ca	-0.67	-10.89	51.02	Xi33	1996.5	100% An	-5.19	-20.39	121.73
Wu64	2067.4	100% An	-5.50	-17.39	94.64	Xi34	1993.2	100% An	-4.00	-19.22	110.45
Wu64	2068.35	60% An+40% Ca	-4.77	-17.79	97.94	Xi53	2013	100% An	-3.98	-19.82	116.12
Wu64	2084.7	100% An	-0.66	-19.12	109.55	Xi53	2012	100% An	-4.82	-20.09	118.73
Wu64	2074.5	100% An	-6.52	-19.41	112.22	Xi55	2017.4	95% Ca+5% Fc	-9.63	-16.62	74.17
Wu64	2086.2	100% An	-5.68	-19.66	114.63	Xi58	2135.5	100% An	-6.21	-18.59	104.79
Wu64	2089.8	100% An	-4.06	-20.02	118.06	Zhen383	2279	70% An+25% Ca +5% Do	-7.68	-17.34	94.25
Wu64	2078.8	100% An	-5.66	-20.05	118.35	Zhen383	2272.2	95% An+5% Ca	-6.72	-19.42	112.31
Wu64	2081.7	40% An+30% Ca+30% Do	-5.41	-20.36	121.42	Zhen383	2305.95	95% An+5% Ca	-1.34	-20.72	125.09
Wu64	2084.1	95% An+5% Ca	-2.34	-20.39	121.74	Zhen383	2302.8	95% An+5% Ca	-6.61	-20.74	125.31
Wu64	2072	100% An	-8.12	-20.69	124.79	Zhen383	2283.47	95% An+5% Do	-5.12	-20.77	125.63
Wu64	2070.5	95% An+5% Do	-8.21	-20.91	127.11	Zhen383	2303.85	80% An+15% Ca +5% Do	-2.58	-21.18	129.95
Wu64	2079.7	60% An+40% Do	-9.85	-21.04	128.41	Zhen383	2300	100% An	-2.80	-21.40	132.32
Wu64	2081.2	90% An+10% Fc	-7.40	-21.50	133.38	Zhen383	2272.35	85% Fc+15% An	-4.11	-19.16	95.11
Wu64	2091.3	40% An+30% Ca+30% Do	-2.96	-22.11	140.32	Zhen383	2278.6	100% Fc	-6.14	-20.13	104.07
Wu64	2073.4	60% Fc+40% An	-5.19	-20.18	104.58	Zhen383	2280.42	95% Fc+5% An	-0.80	-20.75	110.20
Wu64	2089.1	75% Fc+25% An	-4.88	-20.20	104.74	Zhen383	2299.5	100% Fc	-6.32	-21.23	115.18
Wu64	2076.3	100% Fc	-5.04	-19.59	99.03	Zhen383	2278	90% Ca+10% Do	-10.23	-16.35	72.14
Xi128	1987.55	100% An	-5.05	-19.47	112.79	Zhen383	2302.36	95% Ca+5% An	-6.66	-20.78	110.57
Xi128	1986.45	100% An	-7.77	-20.84	126.38	Zhen383	2285.15	80% Do+15% Ca +5% Fc	-9.62	-13.14	64.29
Xi17	2148.4	100% Fc	-4.20	-20.58	108.48	Zhuang20	1848	100% An	-6.08	-19.78	115.77
Xi180	2112.1	100% Fc	-5.08	-19.61	99.16						

815

Note: The formula used in calculating calcite mineral temperature is $1000\ln\alpha_{\text{calcite-water}} = 2.78 \times 10^6/T^2 - 2.89$ (Friedman and

816

O'Neil, 1977); the formula used in calculating dolomite mineral temperature is $1000\ln\alpha_{\text{dolomite-water}} = 3.06 \times 10^6/T^2 - 3.24$

817

(Matthews and Katz, 1977); $1000\ln\alpha_{\text{carbonate-water}} = \delta^{18}\text{O}_{\text{carbonate}} - \delta^{18}\text{O}_{\text{water}}$; and $\delta^{18}\text{O}_{\text{SMOW}} (\text{‰}) = 1.03091\delta^{18}\text{O}_{\text{PDB}} + 30.91$ (Coplen,

818

et al., 1983).

Microthermometric data of the aqueous fluid inclusions in Chang 8 member tight sandstone reservoirs.

Well	Depth, m	Host mineral	Size, µm	types	Th, °C	Tm, ice/°C	Salinity, NaCl wt.% equiv.(from Bodnar,1993)	Well	Depth,m	Host mineral	Size, µm	types	Th, °C	Tm, ice/°C	Salinity, NaCl wt.% equiv.(from Bodnar,1993)
Wu121	2087.9	Carbonate cement	3×8	Aqueous	56.4	-4.8	7.59	Xi23	2095	Carbonate cement	2×4	Aqueous	68.3	-2.9	4.80
Wu121	2087.9	Carbonate cement	2×2	Aqueous	68.5	-4.3	6.88	Xi23	2095	Carbonate cement	2×2	Aqueous	54.8	-2.6	4.34
Wu121	2087.9	Quartz overgrowth	2×2	Aqueous	104.3	-5.1	8.00	Xi23	2095	Quartz overgrowth	4×7	Aqueous	106	-4.6	7.31
Wu64	2081.2	Carbonate cement	2×10	Aqueous	54.2	-4.7	7.45	Xi23	2095	Carbonate cement	2×3	Aqueous	81.6	-2.5	4.18
Wu64	2081.2	Carbonate cement	2×4	Aqueous	63.9	-4.9	7.73	Xi23	2095	Quartz overgrowth	3×5	Aqueous	112	-14.5	18.22
Wu64	2081.2	Quartz overgrowth	2×2	Aqueous	99.7	-5.2	8.14	Xi23	2095	Quartz overgrowth	5×9	Aqueous	119	-5.6	8.68
Wu64	2081.2	Quartz overgrowth	2×5	Aqueous	102.8	-4.5	7.17	Xi23	2095	Quartz overgrowth	2×5	Aqueous	120	-10.7	14.67
Xi128	1987.55	Quartz overgrowth	2×3	Aqueous	88.6	-4.2	6.74	Xi32	1940	Quartz overgrowth	3×6	Aqueous	85.9	-3.9	6.30
Xi128	1987.55	Quartz overgrowth	2×6	Aqueous	95.8	-4.3	6.88	Xi32	1940	Quartz overgrowth	2×2	Aqueous	86.5	-4.2	6.74
Xi17	2148.4	Authigenic quartz	3×5	Aqueous	71	-12.9	16.80	Xi32	1940	Quartz overgrowth	3×3	Aqueous	89.3	-4.6	7.31
Xi17	2148.4	Quartz overgrowth	2×12	Aqueous	77.3	-13.1	16.99	Xi33	1996.5	Quartz overgrowth	3×5	Aqueous	96.5	-9.1	12.96
Xi17	2148.4	Quartz overgrowth	5×6	Aqueous	82.5	-14.5	18.22	Xi33	1996.5	Quartz overgrowth	2×2	Aqueous	98.4	-4.1	6.59
Xi17	2148.4	Authigenic	3×10	Aqueous	90	-8.9	12.73	Xi33	1996.5	Carbonate	2×4	Aqueous	51.7	-3.4	5.56

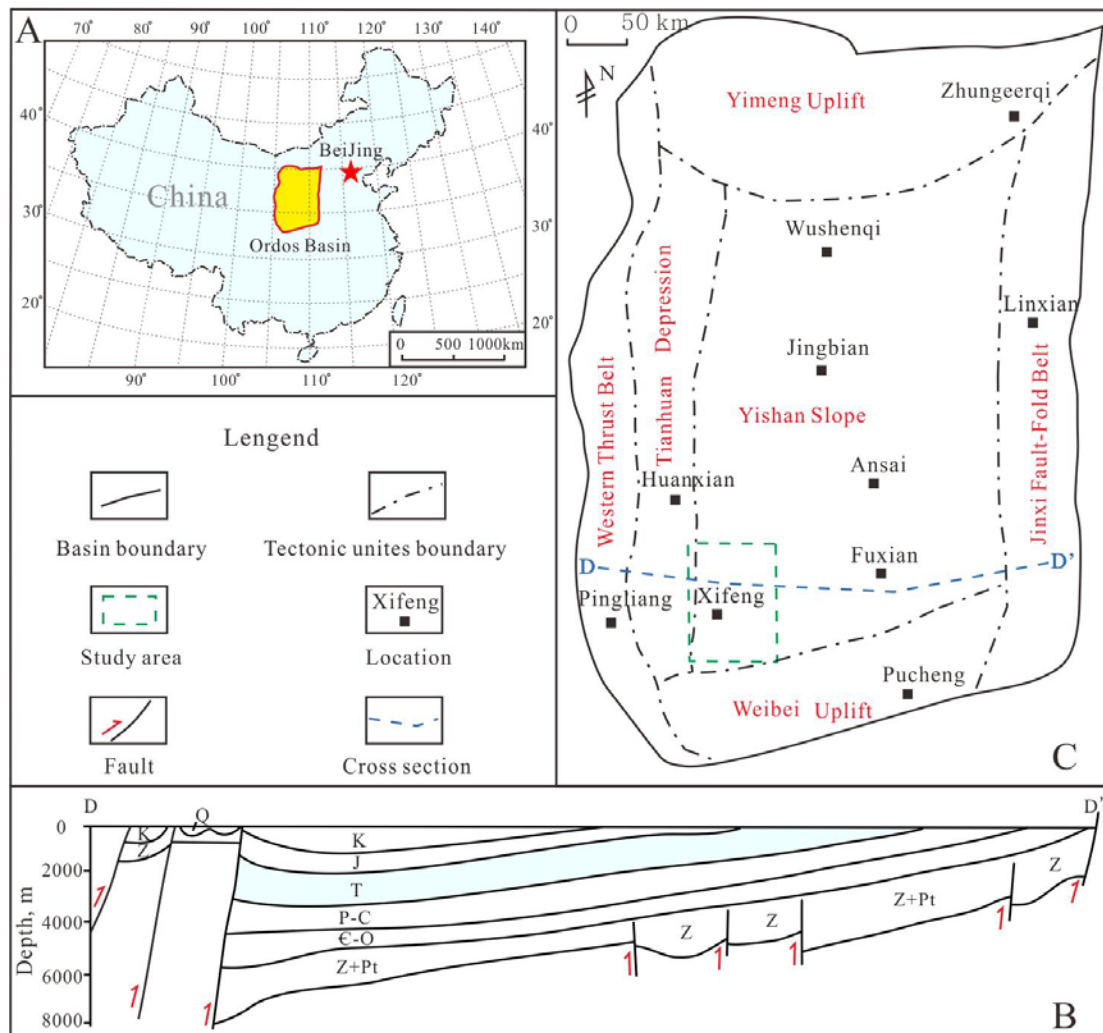
		quartz								cement					
Xi17	2148.4	Carbonate	2×2	Aqueous	68.5	-10.9	14.87	Xi34	1993.2	Carbonate	2×6	Aqueous	63.4	-16.2	19.60
		cement								cement					
Xi17	2148.4	Quartz	2×3	Aqueous	121	-11.5	15.47	Xi34	1993.2	Carbonate	2×5	Aqueous	68.6	-15.4	18.96
		overgrowth								cement					
Xi180	2112.1	Quartz	3×6	Aqueous	79.2	-5.3	8.28	Xi53	2013	Quartz	2×4	Aqueous	120.4	-12.1	16.05
		overgrowth								overgrowth					
Xi180	2112.1	Quartz	2×5	Aqueous	80.7	-7.9	11.58	Xi55	2017.4	Quartz	3×4	Aqueous	93.5	-8.4	12.16
		overgrowth								overgrowth					
Xi180	2112.1	Quartz	3×5	Aqueous	83.7	-9.2	13.07	Xi55	2017.4	Carbonate	2×6	Aqueous	63.3	-8.9	12.73
		overgrowth								cement					
Xi180	2112.1	Quartz	3×5	Aqueous	108.5	-8.7	12.51	Xi55	2017.4	Quartz	3×8	Aqueous	97.6	-9.3	13.18
		overgrowth								overgrowth					
Xi180	2112.1	Quartz	2×3	Aqueous	121.8	-17.6	20.67	Xi58	2135.5	Carbonate	2×2	Aqueous	66.2	-8.2	11.93
		overgrowth								cement					
Xi200	2202.5	Carbonate	2×6	Aqueous	62.8	-16.3	19.68	Xi58	2135.5	Quartz	2×5	Aqueous	97.9	-9.5	13.40
		cement								overgrowth					
Xi200	2202.5	Carbonate	2×8	Aqueous	64.6	-16.9	20.15	Xi58	2135.5	Quartz	3×3	Aqueous	101.5	-4.8	7.59
		cement								overgrowth					
Xi200	2202.5	Carbonate	2×8	Aqueous	106.5	-15.1	18.72	Zhen383	2302.36	Carbonate	3×10	Aqueous	54.2	-16.8	20.07
		cement								cement					
Xi200	2202.5	Carbonate	2×6	Aqueous	108.4	-15.8	19.29	Zhen383	2302.36	Carbonate	2×6	Aqueous	109.3	-15.7	19.21
		cement								cement					
Xi200	2202.5	Carbonate	2×10	Aqueous	109.1	-15.5	19.05	Zhen383	2302.36	Carbonate	3×4	Aqueous	114.6	-15.5	19.05
		cement								cement					
Xi203	1873.6	Carbonate	2×2	Aqueous	56.7	-9.4	13.29	Zhen383	2302.36	Carbonate	3×8	Aqueous	117.8	-16.3	19.68
		cement								cement					
Xi211	1780.5	Quartz	2×3	Aqueous	92.4	-3.9	6.30	Zhuang20	1848	Quartz	2×2	Aqueous	90.3	-8.4	12.16
		overgrowth								overgrowth					
Xi211	1780.5	Quartz	2×5	Aqueous	94.1	-3.6	5.86	Zhuang20	1848	Quartz	3×10	Aqueous	93.2	-7.9	11.58
		overgrowth								overgrowth					

Xi220	1943.7	Quartz overgrowth	2×4	Aqueous	85.9	-2.1	3.55	Zhuang20	1848	Carbonate cement	3×5	Aqueous	65.7	-8.1	11.81
Xi220	1943.7	Quartz overgrowth	2×7	Aqueous	86.7	-2.9	4.80	Zhuang20	1848	Carbonate cement	2×6	Aqueous	66.4	-8.8	12.62
Xi220	1943.7	Quartz overgrowth	2×2	Aqueous	88.2	-2.6	4.34	Zhuang52	1953.5	Quartz overgrowth	2×3	Aqueous	117.8	-6.7	10.11
Xi220	1943.7	Carbonate cement	3×5	Aqueous	64.8	-2.5	4.18	Zhuang52	1953.5	Quartz overgrowth	2×5	Aqueous	123.5	-16.9	20.15
Xi23	2095	Carbonate cement	2×5	Aqueous	55.5	-2.3	3.87	Zhuang53	2013	Quartz overgrowth	2×4	Aqueous	96.7	-10.1	14.04

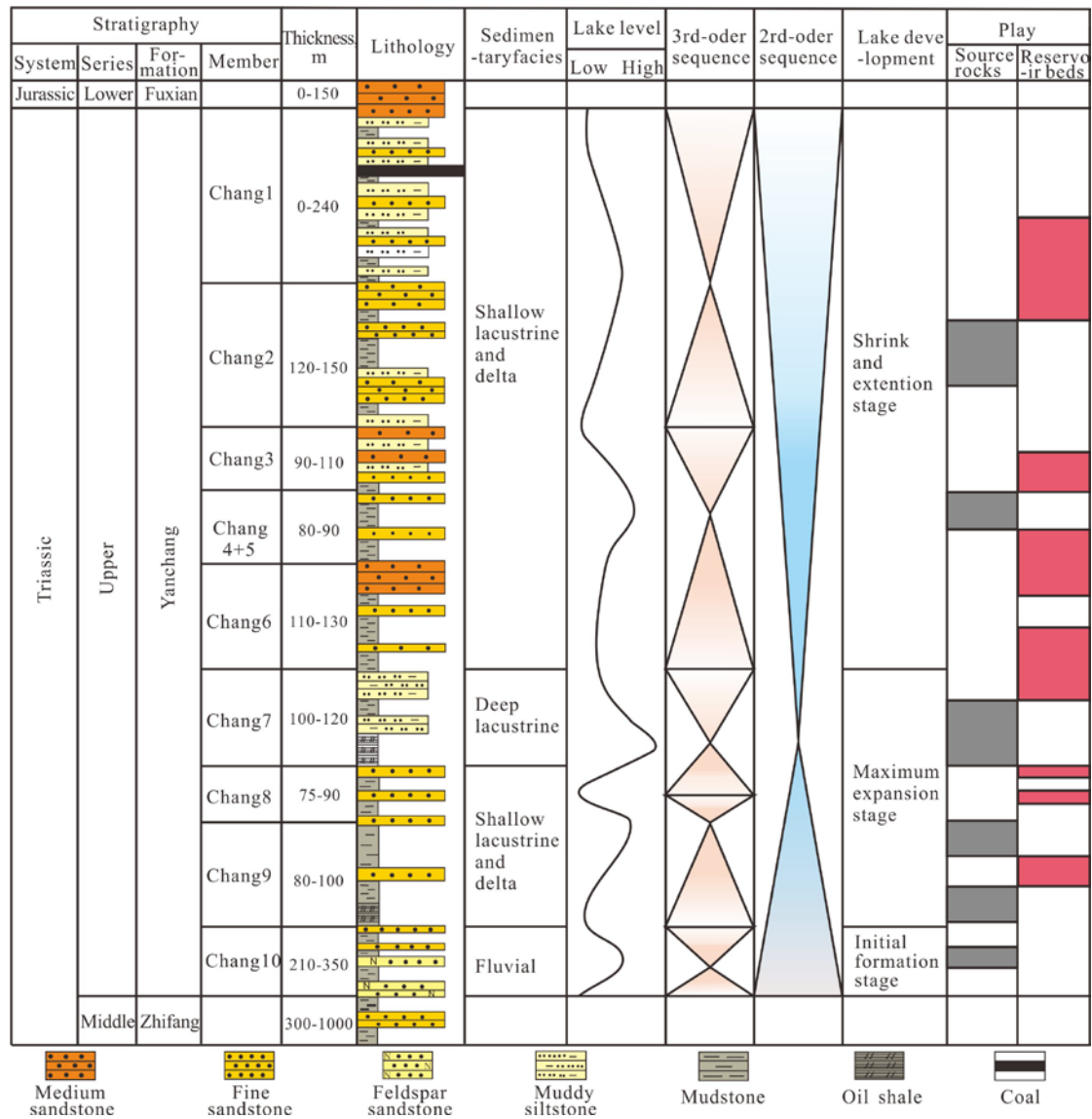
Note: The formula used in calculating salinity is $S=0.00+1.78T-0.0442T^2+0.000557T^3$ (Bodnar, 1993); T_h -homogenization temperature; T_m -final ice melting temperature

821
822
823
824
825
826
827
828
829
830
831
832
833
834
835
836
837
838
839
840

841 **Figure captions**

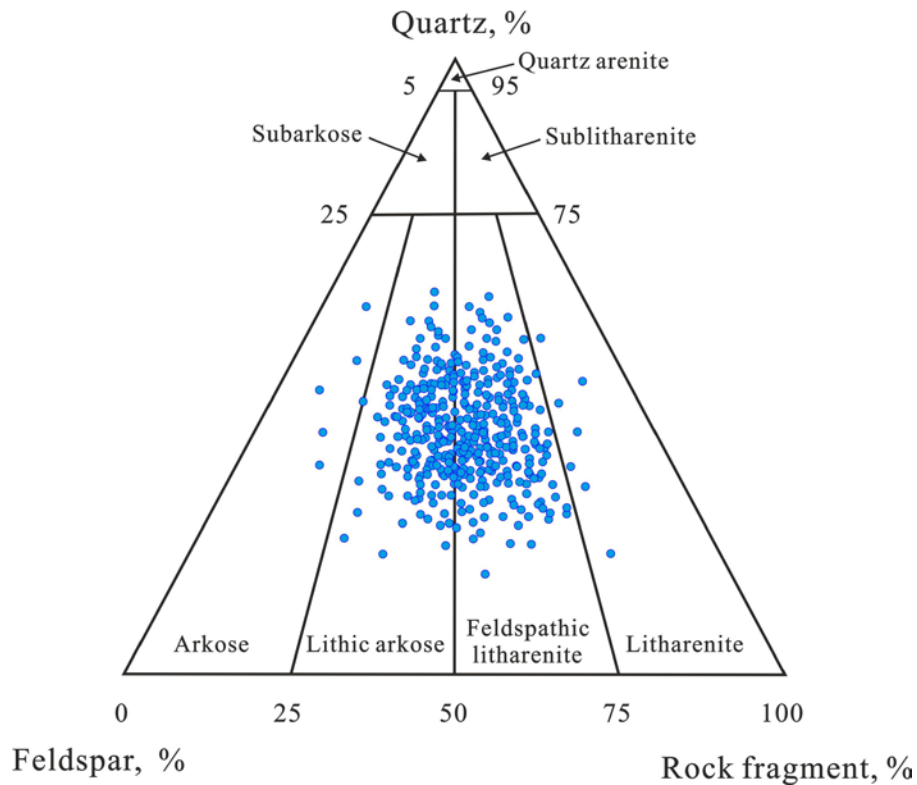


842
 843 **Figure 1.** (A) Location map of the Ordos Basin, China. (B) Cross-section (DD' in
 844 Figure 1C) of the Ordos Basin showing the various tectonic units and strata (Triassic
 845 rocks in blue). (C) Simplified tectonic units and location map of the Xifeng Area in
 846 the Ordos Basin (modified from Liu et al., 2016).



847

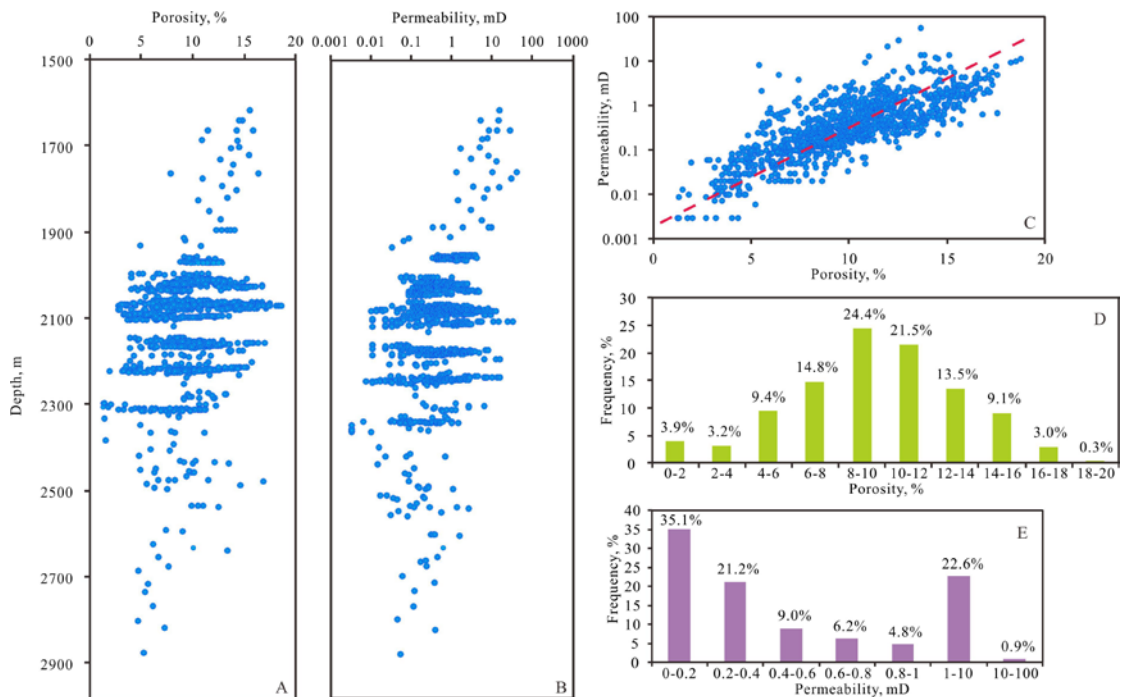
848 **Figure 2.** The composite stratigraphic columns of the Yanchang Formation in Ordos
 849 Basin, showing the evolutions of lake level, lake development and sedimentary facies
 850 and the major elements of tight sandstone hydrocarbon reservoir (modified from Zhou
 851 et al., 2016 and Xu et al., 2017).



852

853 **Figure 3.** Rock composition of the Chang 8 Member tight sandstone of Yanchang

854 Formation in the Xifeng Area plotted on Folk's (1974) ternary diagram.

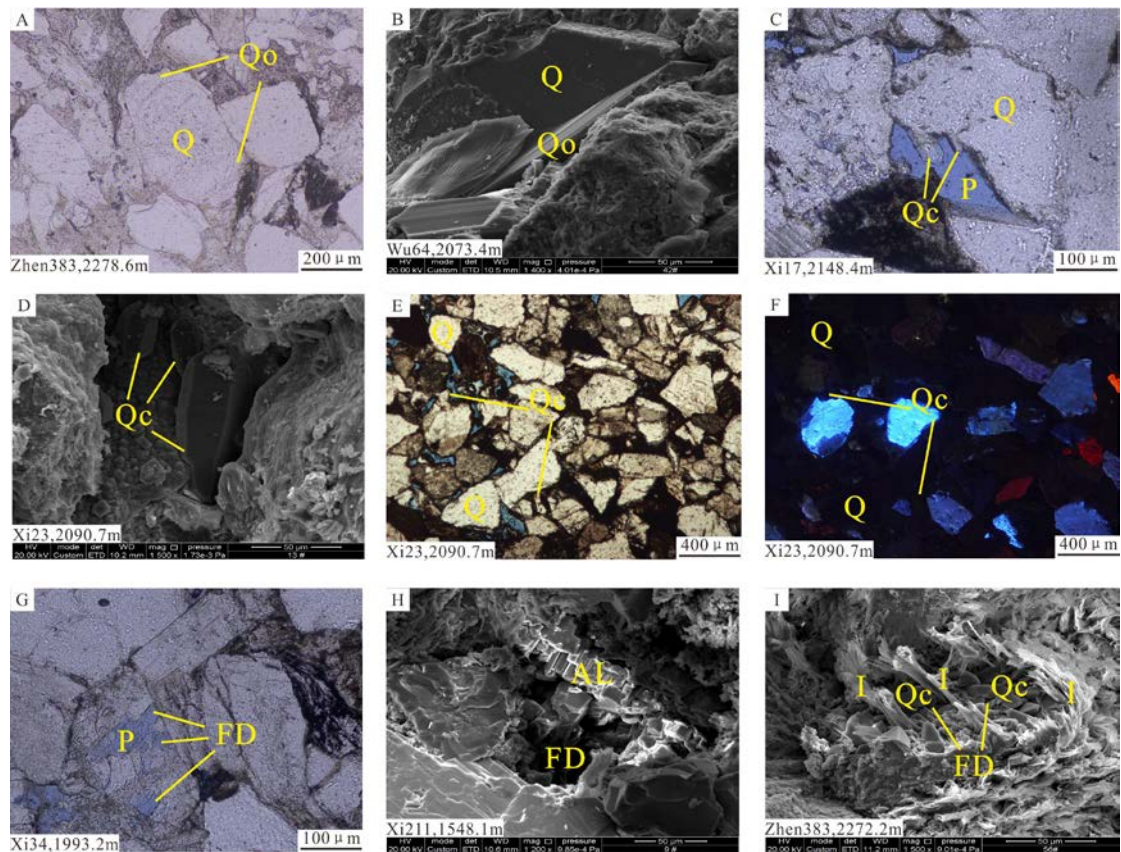


855

856 **Figure 4.** Characteristics of Chang 8 Member tight sandstone reservoir properties in

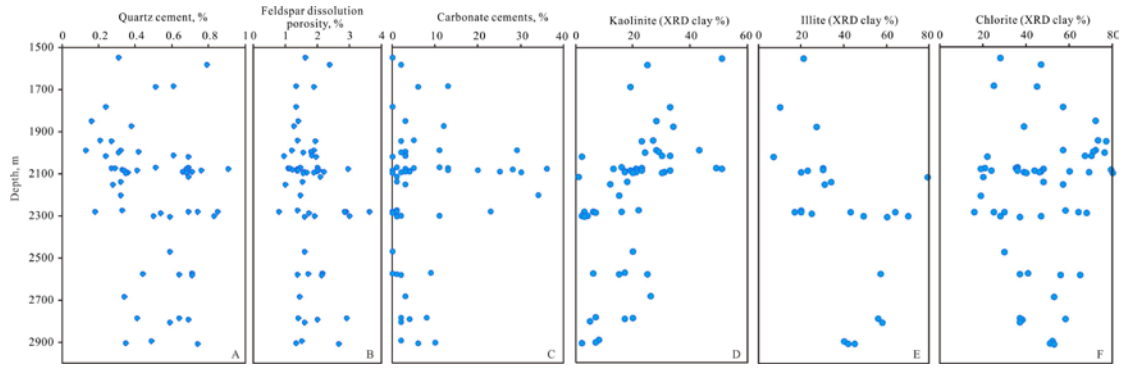
857 Xifeng Area: (A) Porosity versus depth. (B) Permeability versus depth. (C) Porosity

858 versus permeability. (D) Porosity distribution. (E) Permeability distribution.



859

860 **Figure 5.** Characteristics of quartz cements and feldspar dissolution in Chang 8
 861 Member tight sandstone reservoirs (pore space is shown in blue). (A) Micrograph of
 862 thin section showing the quartz overgrowth. (B) Micrograph of SEM showing the
 863 quartz overgrowth. (C) Micrograph of thin section showing the authigenic quartz
 864 crystal. (D) Micrograph of SEM showing the authigenic quartz crystal. (E)
 865 Micrograph of thin section showing the authigenic quartz crystal. (F) Idem with E but
 866 micrograph of CL. (G) Micrograph of thin section showing feldspar partly dissolved.
 867 (H) Micrograph of SEM showing feldspar dissolution and authigenic albite. (H)
 868 Micrograph of SEM showing feldspar dissolution, authigenic quartz crystal and
 869 authigenic fibrous illite. Q-Quartz detrital grain; Qo-Quartz overgrowth; Qc-Quartz
 870 crystal; P- Pores; FD-Feldspar dissolution; AL-Albite; I-Illite.



871

872 **Figure 6.** Vertical distribution characteristics of quartz cement (A), feldspar
 873 dissolution porosity (B), carbonate cements (C), kaolinite (D), illite (E) and chlorite (F)
 874 in Chang 8 Member tight sandstone reservoirs, Xifeng Area.

875

876

877

878

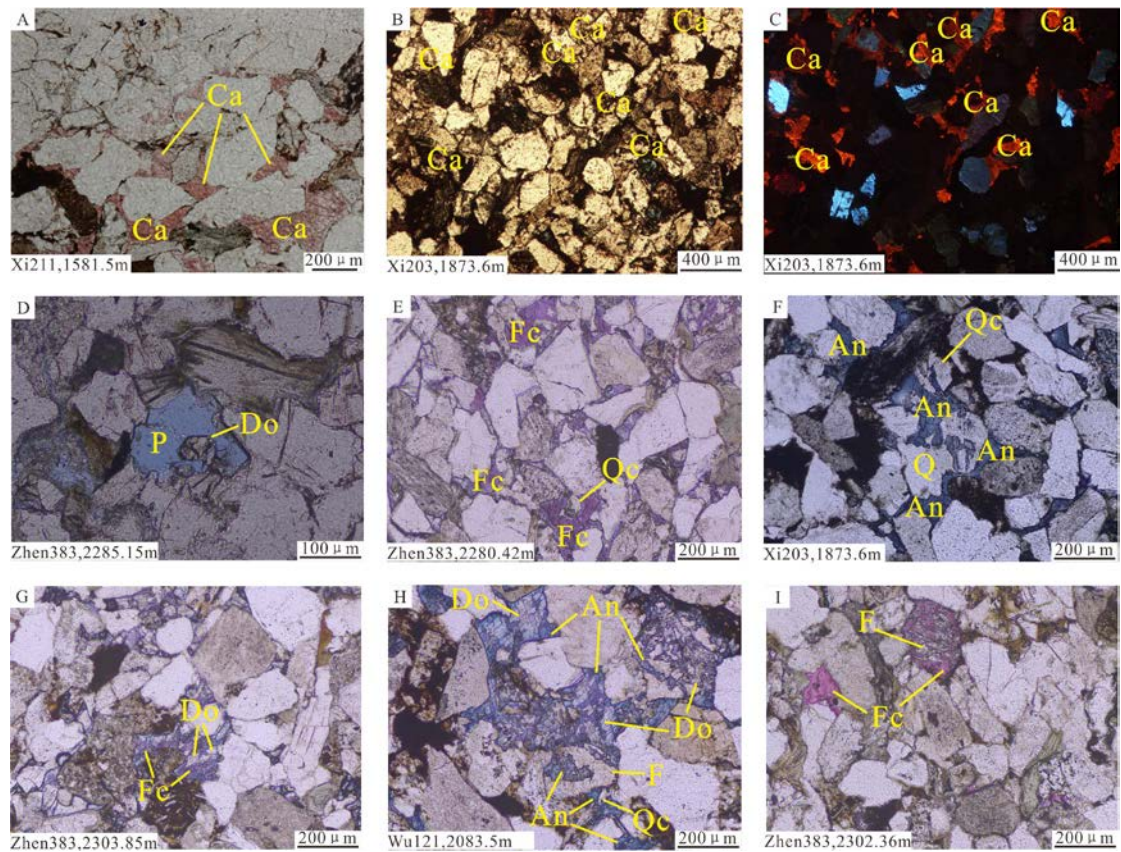
879

880

881

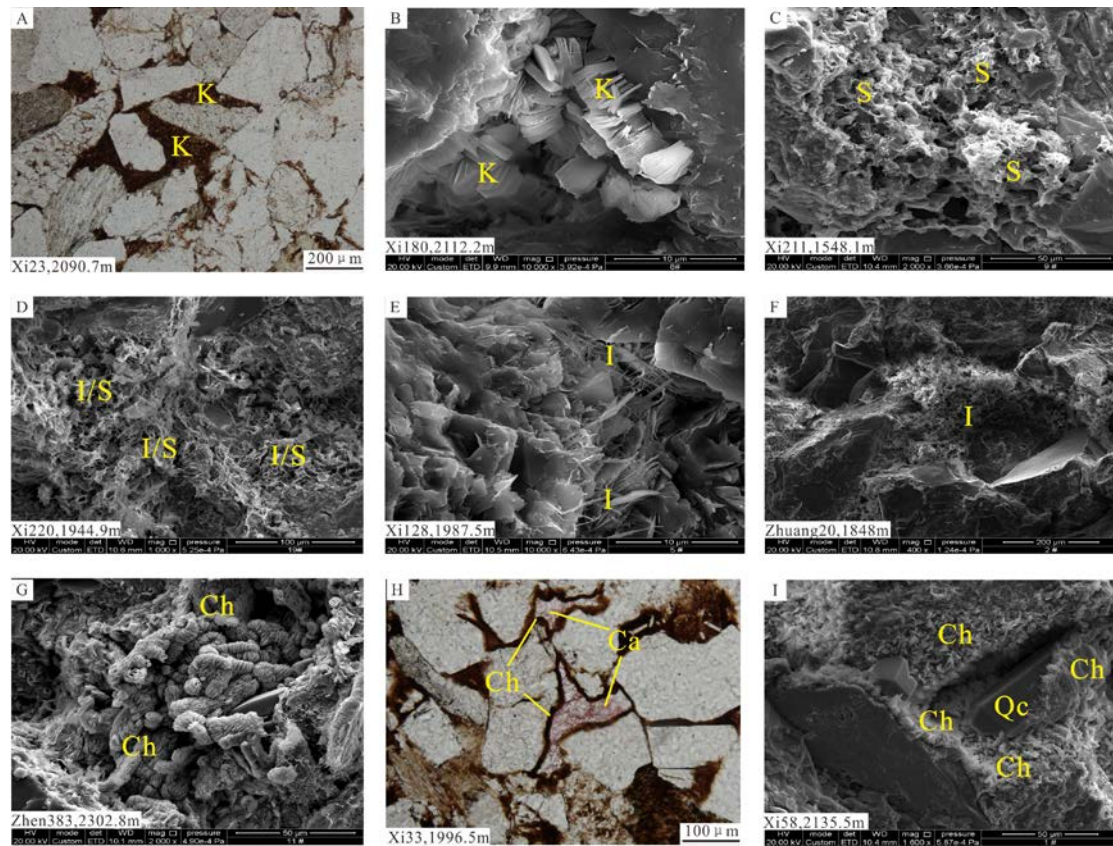
882

883



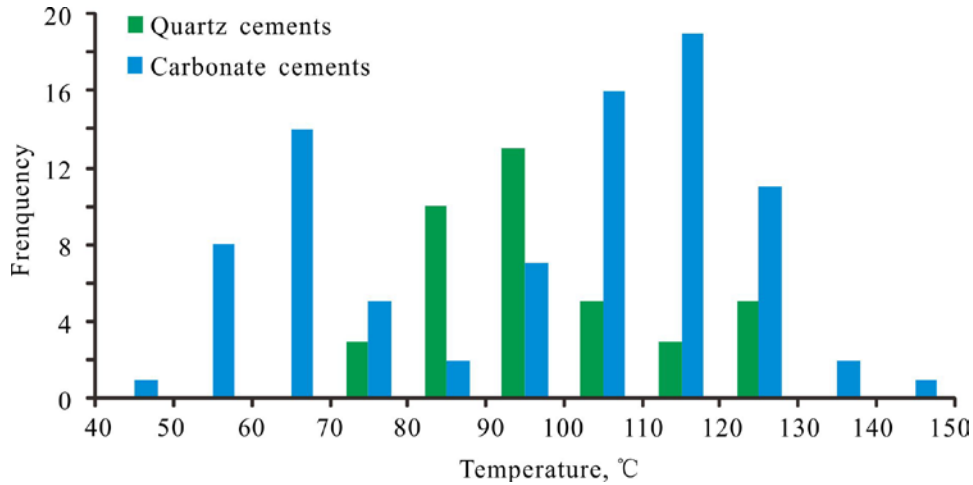
884

885 **Figure 7.** Characteristics of carbonate cements in Chang 8 Member tight sandstone
 886 reservoirs. (A) Micrograph of thin section showing the pore-filling calcite cement. (B)
 887 Micrograph of thin section showing the pore-filling calcite cement. (C) Idem with B
 888 but micrograph of CL. (D) Micrograph of thin section showing the euhedral rhombs
 889 of dolomite cement partly filling the intergranular pore. (E) Micrograph of thin
 890 section showing the ferrocalcite cements around the euhedral quartz crystal. (F)
 891 Micrograph of thin section showing the ankerite cements around the euhedral quartz
 892 crystal and partly replacing quartz grain. (G) Micrograph of thin section showing the
 893 ferrocalcite cements partly replacing dolomite cements. (H) Micrograph of thin
 894 section showing the ankerite cements partly replacing dolomite cements and
 895 completely filling feldspar dissolution pore. (I) Micrograph of thin section showing
 896 the ferrocalcite cements completely filling feldspar dissolution pore. Q-Quartz detrital
 897 grain; Qc-Quartz crystal; P- Pores; F-Feldspar; Ca-Calcite; Do-Dolomite;
 898 Fc-Ferrocalcite; An-Ankerite.



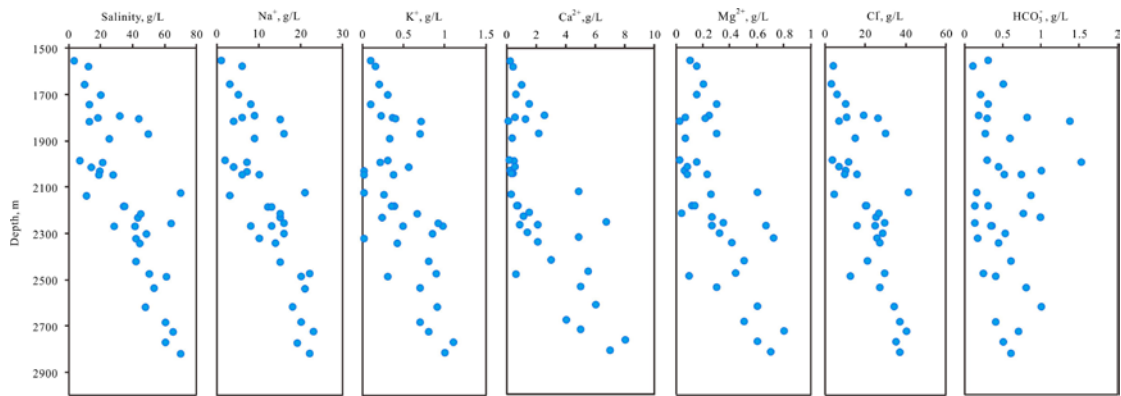
899

900 **Figure 8.** Characteristics of clay cements in Chang 8 Member tight sandstone
 901 reservoirs. (A) Micrograph of thin section showing pore-filling kaolinite. (B)
 902 Micrograph of SEM showing authigenic vermicular kaolinite. (C) Micrograph of
 903 SEM showing authigenic curly flaky smectite. (D) Micrograph of SEM showing
 904 authigenic honeycomb I/S. (E) Micrograph of SEM showing authigenic fibrous illite.
 905 (F) Micrograph of SEM showing authigenic honeycomb illite. (G) Micrograph of
 906 SEM showing authigenic rosette-shaped chlorite. (H) Micrograph of thin section
 907 showing authigenic chlorite rim covering detrital grain. (I) Micrograph of SEM
 908 showing authigenic needle chlorite coating covering authigenic quartz crystal.
 909 Ca-Calcite; Qc-Quartz crystal; K-Kaolinite; S-Smectite; I/S-mixed-layer
 910 illite/smectite; I-Illite; Ch-Chlorite.



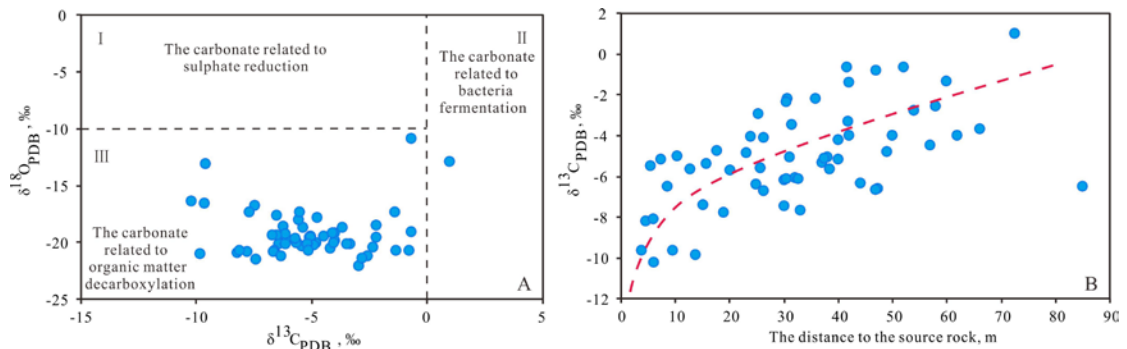
911

912 **Figure 9.** Comparison of the homogenization temperatures of the aqueous inclusions
 913 in quartz cements and carbonate cements (including the approximate carbonate
 914 cements precipitation temperatures are calculated by oxygen isotope) in Chang 8
 915 Member tight sandstone reservoirs.



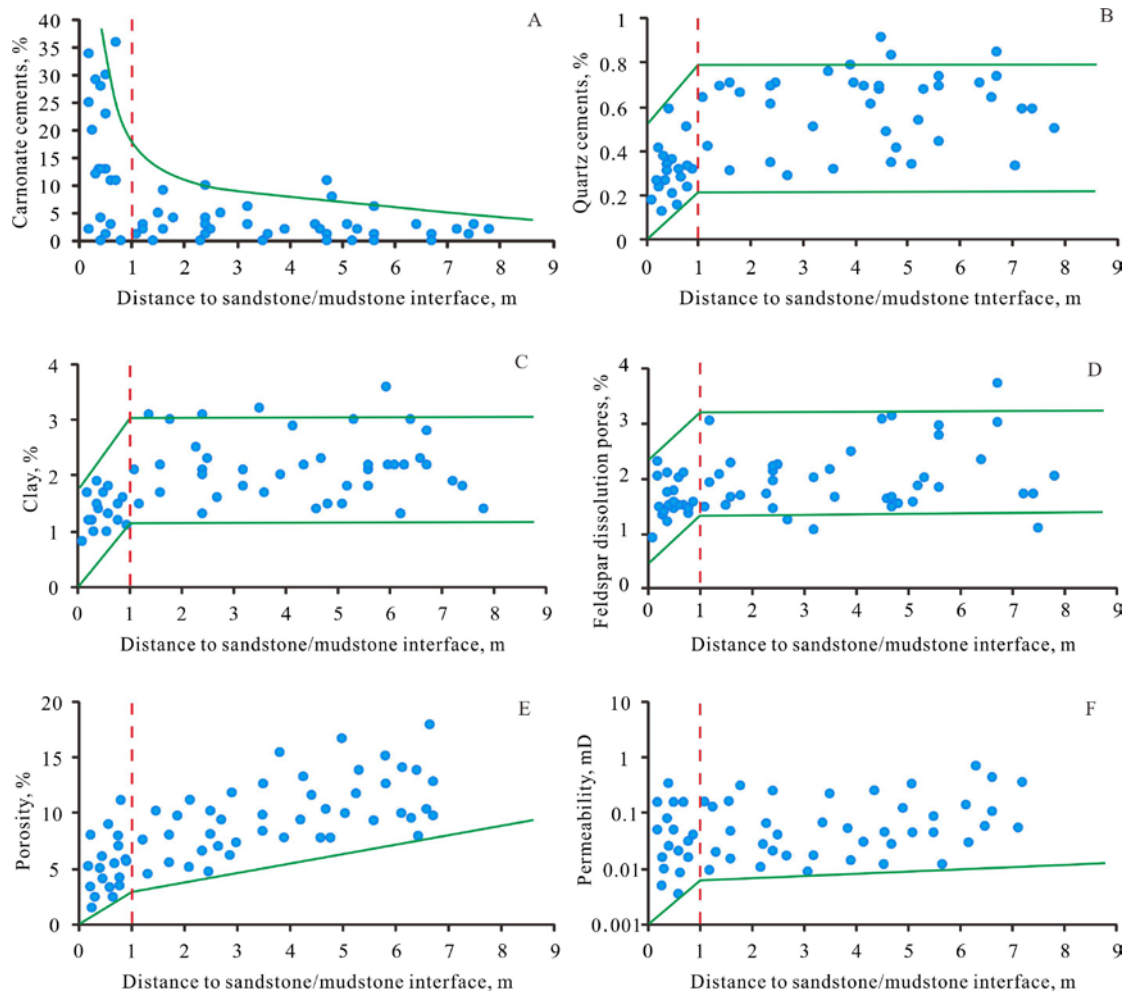
916

917 **Figure 10.** Salinity and concentration of different ions in pore water from Chang 8
 918 Member tight sandstone in Xifeng Area.



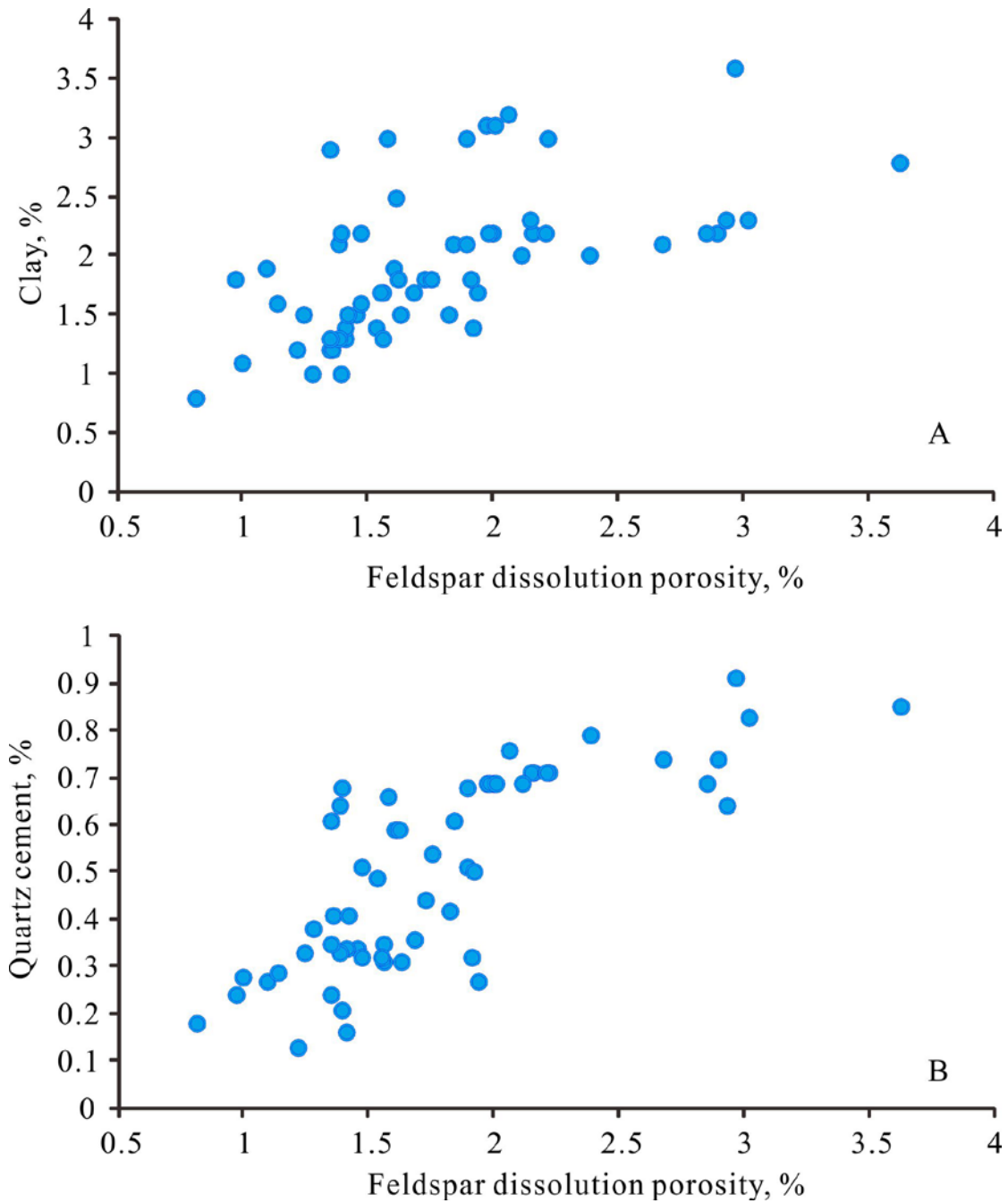
919

920 **Figure 11.** The distribution characteristics of isotopes. (A) Introduction of carbonate
 921 and oxygen isotope distribution (modified from Irwin et al., 1977; Xi et al., 2015a). (B)
 922 $\delta^{13}\text{C}$ values increase with the increasing distance of samples to source rocks.



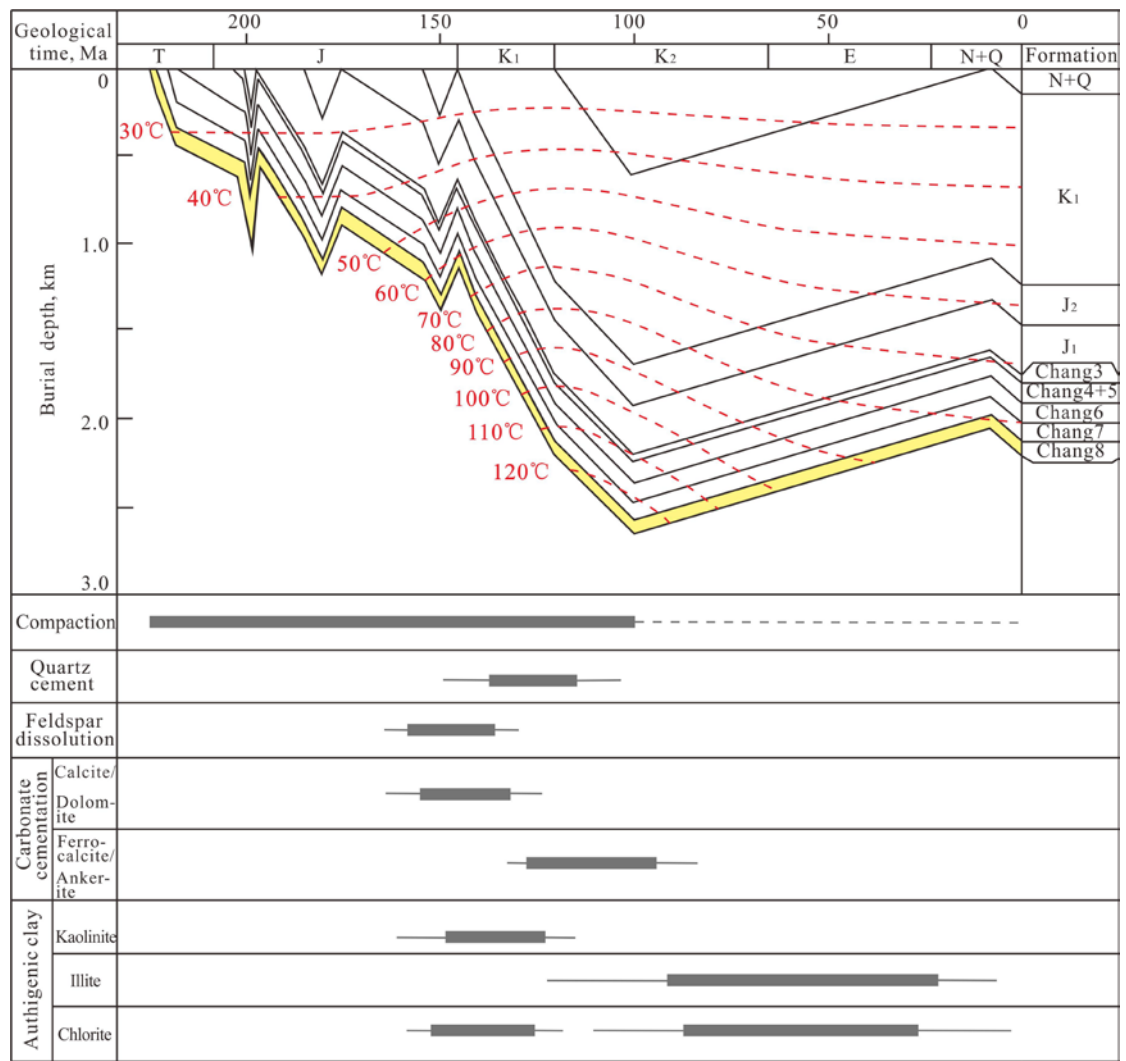
923

924 **Figure 12.** Relationship between sandstone reservoir quality and the distance to
 925 sandstone/mudstone interface. (A) Cross-plot between the content of carbonate
 926 cements and the distance to sandstone/mudstone interface. (B) Cross-plot between the
 927 content of quartz cements and the distance to sandstone/mudstone interface. (C)
 928 Cross-plot between the content of clay minerals and the distance to
 929 sandstone/mudstone interface. (D) Cross-plot between the feldspar dissolution pores
 930 and the distance to sandstone/mudstone interface. (E) Cross-plot between the porosity
 931 and the distance to sandstone/mudstone interface. (F) Cross-plot between the
 932 permeability and the distance to sandstone/mudstone interface.



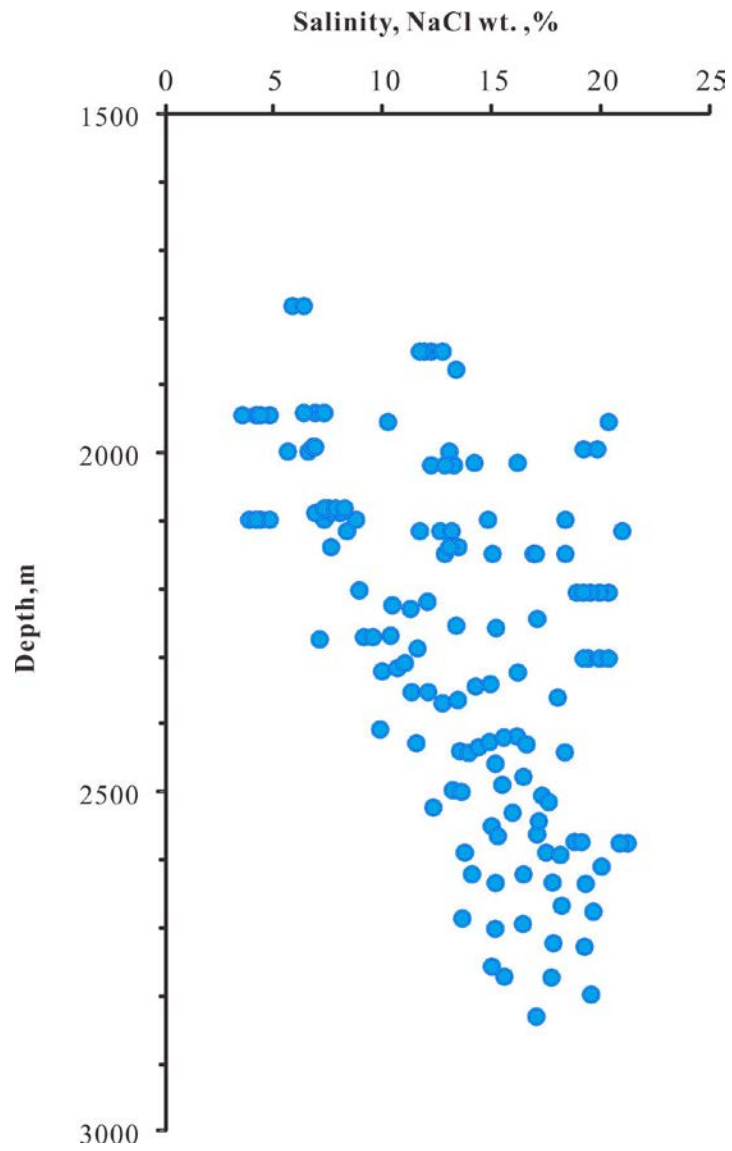
933

934 **Figure 13.** Relationship between the content of feldspar dissolution porosity,
 935 authigenic clay (A) and quartz cement (B) in Chang 8 Member tight sandstone in
 936 Xifeng Area.



937

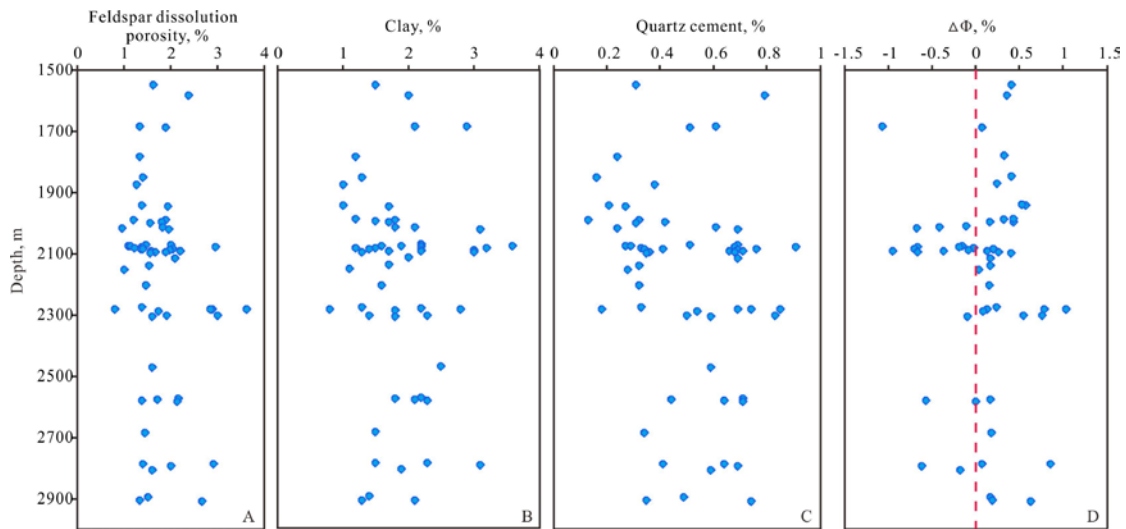
938 **Figure 14.** Burial-thermal history and diagenetic sequence of the Chang 8 Member
 939 tight sandstone reservoirs in Xifeng Area.



940

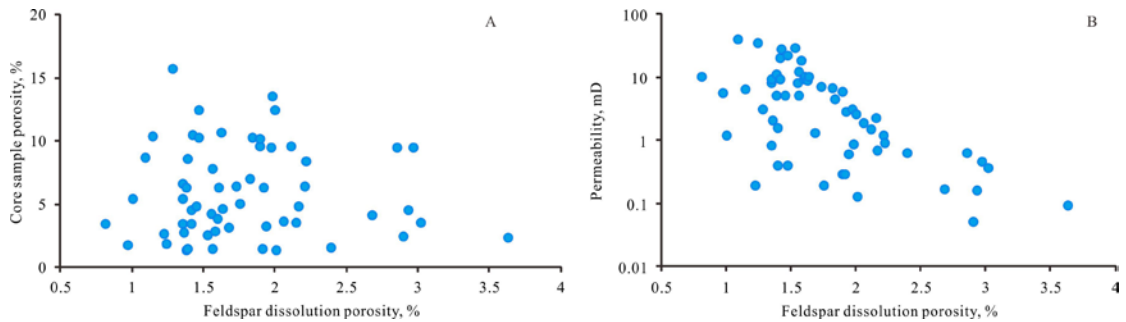
941 **Figure 15.** Vertical variation of salinity from ice melting temperature of aqueous fluid
942 inclusions of Chang 8 Member tight sandstone in Xifeng Area.

943



944

945 **Figure 16.** The vertical distribution of the content of feldspar dissolution porosity (A),
 946 clay (B) and quartz cement (C) and their difference values (D) in thin section of
 947 Chang 8 Member tight sandstone in Xifeng Area. $\Delta\Phi$ - Difference values between
 948 feldspar dissolution porosity and feldspar dissolved byproducts (The calculation
 949 method was described by Yuan et al. 2015b).



950

951 **Figure 17.** Relationship between the feldspar dissolution porosity, core sample
 952 porosity (A) and core sample permeability (B) in Chang 8 Member tight sandstone in
 953 Xifeng Area.